Effect of DERs on the Voltage Stability of Transmission Systems using a Voltage Stability Index

Sagar Karki

Thesis submitted to the Faculty of the Virginia Polytechnic Institute and State University in partial fulfillment of the requirements for the degree of

Master of Science
in
Electrical Engineering

Robert P. Broadwater, Chair

Virgilio A. Centeno

Jaime De La Reelopez

December 10, 2020
Blacksburg, Virginia

Keywords: Voltage Stability, Stability Margin, Distributed Energy Resources, Resiliency, Transmission Planning, etc.

Effect of DERs on the Voltage Stability of Transmission System using a Voltage Stability Index

Sagar Karki

(ABSTRACT)

Interconnection of DERs into the transmission lines is starting to take a substantial share of the total power capacity. Although the largest share of power generation attributes to coal and gas power plants, renewable energy is gradually increasing. However, in the past, the size of DERs was relatively smaller, and rooftop PV was the dominant renewable energy source. As a result, the studies for interconnection focused on those rooftop PVs on the distribution side. Since the scenario is slowly changing as more utilities increase the share of clean energy by building large-scale solar farms and wind farms, it is necessary to study the effect of those DERs in the transmission system. Among the various issues, this work focuses on the impact on a transmission system's voltage stability. When the voltage stability at a point in the system is compromised, it can affect the entire power system's overall security, quality, and reliability. Therefore, this work aims to assess the system's stress due to increased loading conditions and increased growth of DERs integration. A steady-state voltage stability index is used to generate a heat-map that identifies the areas where the system can go unstable in events like the loss of the renewable generation under a bus. The steady-state simulation is performed on the IEEE 14 bus system in Distributed Engineering Workstation (DEW) to find the system's weak links using the stability heat-map. DERs are added to the corresponding weak buses, and the improvement in the stability margin for various penetration levels are studied. The results obtained from the steady-state analysis are also verified using the dynamic simulation of the model using OpenModelica.

Effect of DERs on the Voltage Stability of Transmission System using a Voltage Stability Index

Sagar Karki

(GENERAL AUDIENCE ABSTRACT)

Transmission networks are going through some of the fundamental changes in how they are planned and operated as more and more renewable energy sources are connected to the grid. Unlike the traditional setup where the transmission line transfers bulk power from a large generator to the load center at a different location, the advent of renewable energy resources enables the power to be generated in distributed form. It allows electrical power to be generated closer to the demand. In the long run, the transmission system's stress reduces as a significant portion of demand is supplied locally. Thus, the distributed energy resources (DERs) in the power grid have the potential for substantial economic and environmental benefits. However, it can also bring about a range of challenges to the power system. Among the various issues, this work focuses on the effects on a transmission system's voltage stability. When the voltage stability at a point in the system is compromised, it can affect the entire power system. Therefore, this work aims to assess the stress on the system due to increased loading conditions and increased growth of DERs integration, utilizing a voltage stability index to identify the areas where the system can go unstable in events like the loss of renewable generation under a bus. The steady-state simulation is performed on the IEEE 14 bus system to find the weak links in the system where DERs can improve the system's stability. The results obtained from the steady-state analysis are verified using the dynamic simulation of the model.

Dedication

To my parents and my wife.

Acknowledgment

I offer my sincere gratitude to my research advisor Dr. Robert Broadwater for his continuous support and guidance throughout my graduate studies at Virginia Tech. Without his thoughtful encouragement and careful supervision, this thesis would never have taken shape. I am highly indebted to Dr. Virgilio Centeno and Dr. Jaime De La Ree for guiding me as my committee members and for their never-ending support since the very beginning of my journey at Virginia Tech.

In addition to my committee members, I want to thank all the professors in the ECE department whose courses helped shape my career interest in power and energy systems. I want to express my appreciation to all my fellow graduate students in the Power and Energy Center for their co-operation and support whenever needed.

I am forever thankful for my friends and family at Hawthorn--a home away from home. I feel fortunate to have shared a couple of years full of fun with supportive and caring individuals whose memories I will cherish.

I want to thank my parents, whose love and blessings are with me in everything I pursue. No amount of gratitude could ever be enough for the sacrifices they made and their belief in me. I am grateful to my mother-in-law for her constant support and encouragement. Words are not enough to express how lucky I feel to have my wife, Pratigya, in my life, who showers me with love, compassion, and care every single day. She provided me with unfailing support and continuous encouragement throughout my years of study and through the process of researching and writing this thesis. Also, I would like to thank everyone in my family for always supporting me in everything I do.

Contents

List of Figures

List of Tables

1 Introduction

Over several decades, the power system has evolved to form a highly complex system combining large generators, transmission networks, distribution systems, and protective and control equipment. Over time, the dependence on electric power has increased, and therefore the power demand has been continuously growing. This has compelled the system planners to design increasingly larger system networks to meet the demand while maintaining its reliability and security. As a result, the present transmission network has grown to be huge, spread over vast geographical areas, and has become a capital-intensive component of the power system. Therefore, it is undesired to alter the physical configuration of the transmission lines once completed.

The complexity of the network increases as more and more components are added to the system. These networks are designed to operate in the current system configuration and accommodate the gradual increment of load demand and the rapid expansion of grid components. Without proper planning, expansion efforts such as increased load centers can result in unavoidable pressure at undesired locations, causing the system to become unstable.

In addition to the existing challenges in the power system in its traditional setup, the rapid increase in deployment of distributed energy resources in the current grid brings complex issues such as power quality, reliability, and protection issues. It requires appropriate methods for safe integration and reliable operation. The rapid increase can be attributed to environmental concerns and modernization efforts, enhanced by the technological advancements supporting large-scale renewable energy sources. This is an ongoing process posing a challenge to the electrical power system, exacerbated by the rise in penetration level of these resources and complicated by the intermittent nature, mainly in the case of solar and wind generation.

While there is extensive research being conducted concerning the issues such as reduced inertia in the system due to converter interfaced renewable energy resources, optimal placement, sizing of the renewables, and maximum penetration of DERs, there are other issues that can arise in the system after the placement of the renewable energy resources. The issues arise mainly by their loss during the induced momentary cessation and frequency mismatch caused by the disturbances in the system. To this effect, this thesis is focused on analyzing the stress on individual buses due to increased loading conditions that are facilitated by the integration of DERs. Multiple scenarios are explored that can cause instability in the system when it loses DERs during high loading

conditions. The analysis is based on a voltage stability index-based stability margin. This thesis also identifies weak buses in the system using a voltage stability heat map.

This chapter discusses the overview of the power system and its evolution in recent years. It also discusses the challenges that integration of distributed renewable systems pose to the existing system and the prior studies that relate to and motivate this thesis's work. Finally, the objectives of the thesis and some contributions have been presented.

1.1 Prior Works and Motivation

The traditional power system consists of vertically integrated large components. Power generation occurs typically at 11 kV to 33 kV at generation sites, which is stepped up to transmission voltage levels of 69 kV or higher to transfer the power to load centers. A typical transmission system interconnects generating stations and load centers via transformers, transmission lines, and compensating devices, forming the integrated power system [1].

In the last decade, DERs deployment has been significantly increasing on both distribution and transmission grids. While prior efforts were to create an islanded system serving the power from DERs to only the local loads, the trend is shifting towards grid-connected mode. With the decreasing cost of renewables, various energy policy targets according to the regions, creation of a regional market, and the development of advanced control techniques, the rise of renewable integration to the grid will affect the transmission system's operation [2]. This transition necessitates extensive studies on the operation of the system.

Several researchers have focused on voltage stability assessment, including the latest trend of utilizing optimization-based techniques. The use of the Non-linear programming (NLP) approach to place distributed generation and the effect on voltage stability are studied in [3]. But, it doesn't address the natural tendency to an increase in load over time. Authors of [4] have presented an approach for DERs placement in power systems with variable loads to minimize generation cost.

Another aspect of research related to integrating DERs into the grid is finding the maximum penetration level. The high penetration of renewable resources like PV plants can affect the system's steady-state and transient stability due to a vast difference in their characteristics compared to the conventional generation resources [5]. Most of the research on the penetration level of PV is focused on the distribution system, and there is limited research focusing on the penetration levels affecting the transmission systems [6],[7],[8]. Although many of these studies focus on transient voltages being better than

the cases without the PV, they do not consider the actual representation of more extensive, interconnected power systems, nor the effect of the loss of high levels of PV generation.

Of the various issues on the grid due to the addition of large-scale DERs, voltage stability analysis is of considerable concern due to the threat of voltage collapse in the case of the system's inability to maintain voltage after a significant disturbance. [9] explores on voltage stability of renewable sources integrated grid using the continuation power flow method. The analysis considers reduced generation capacity overlooking an existing plant's economic aspect, which may not be effective in actual practice. The authors in [10] have studied the method for maximizing the hosting capacity of DERs using voltage stability on an integrated transmission and distribution system. [11] explores PV generation's impact on an integrated transmission system's voltage stability for different PV penetration levels.

From the system resiliency perspective, author in [12] have studied the inverter-based control scenarios for resiliency improvement of a distribution system. Similarly,[13] discusses the current practices and challenges in system resilience, [14] focuses on uses and mobilization of moveable energy resources for resiliency enhancement. These studies are equally important for the overall system security and reliability performances.

Despite a wide range of research work on the integration of DERs and their various effects on the power system, the impact of renewable resources on the individual bus and its loadability margin lacks a handful of studies. Keeping in mind the increasing penetration of DERs on the transmission system that will eventually result in a 100% renewable grid over time, increasing the challenges to maintain voltage and frequency control, there is a need to support the future load growth with a minimum upgrade in the existing infrastructure. The sustainability can be addressed by properly observing the system- the problem, causes for the problem, and appropriate solutions. Thus, this thesis aims to analyze the stress on individual buses due to increased loading conditions facilitated by the integration of DERs. Multiple scenarios are explored that can make the system unstable because of the loss of the DERs. The analysis is based on a voltage stability index based stability margin using the approach described in [15]. The voltage stability index based stability margin is discussed in section 2.2. Additionally, this thesis identifies weak buses using a heat map based on the stability margin.

The analysis has been performed using the software developed by the former Electrical Distribution Design (EDD) named Distributed Engineering Workstation (DEW) using the Graph Trace Analysis (GTA) based power flow algorithm[11]. The GTA based

approach can solve a substantial composite transmission and distribution system efficiently and accurately[17].

1.2 Objectives and Contributions

This thesis aims to study and assess the system's stress due to increased loading conditions aided by the integration of DERs and identify the situation where the system can go unstable because of the loss of renewable generation using the voltage stability index described in section 2.2. Relative to this objective, the work in this thesis mainly focuses on the following aspects:

- Voltage Stability of a transmission system in the context of varying distributed PV integration and varying load levels as demonstrated in the IEEE 14 bus feeder. The analysis focuses on the relation of PV variability and load variability on a steady-state voltage stability margin. This part of the thesis is conducted in the Distributed Engineering Workstation (DEW) simulation software.
- To compare and validate the analysis of the steady-state representation in the DEW software[18], a dynamic simulation of the same IEEE 14 bus feeder is conducted using the OpenModelica software.

The results of the steady-state voltage stability analysis in DEW are verified with the dynamic simulation results. The study also highlights weak buses in the system using a voltage stability heat map.

1.3 Thesis Organization

The rest of this thesis is outlined as follows. Chapter two discusses this thesis's background, explaining the concept of voltage stability margin and the DEW simulation software. Chapter 3 presents the details on the simulation framework and the setup for different case-studies. It also explains the results from the various case-studies and the comparison between the steady-state and dynamic simulations. Finally, Chapter 4 discusses the conclusions and future directions of the work done in the thesis.

2 Preliminaries

This chapter focuses on the literature review of the background and concepts that the thesis relates to, including the voltage stability margin index used herein, the DEW simulation software, and other relevant topics.

2.1 Power System Stability

Power System Stability is the system's ability to remain in a state of equilibrium during normal operating conditions and return to an acceptable equilibrium state after a disturbance[1]. Based on a range of considerations, power system stability can be classified based on several factors. This section discusses power system stability in terms of voltage, frequency, and rotor angle stability, as organized in [1],[19].

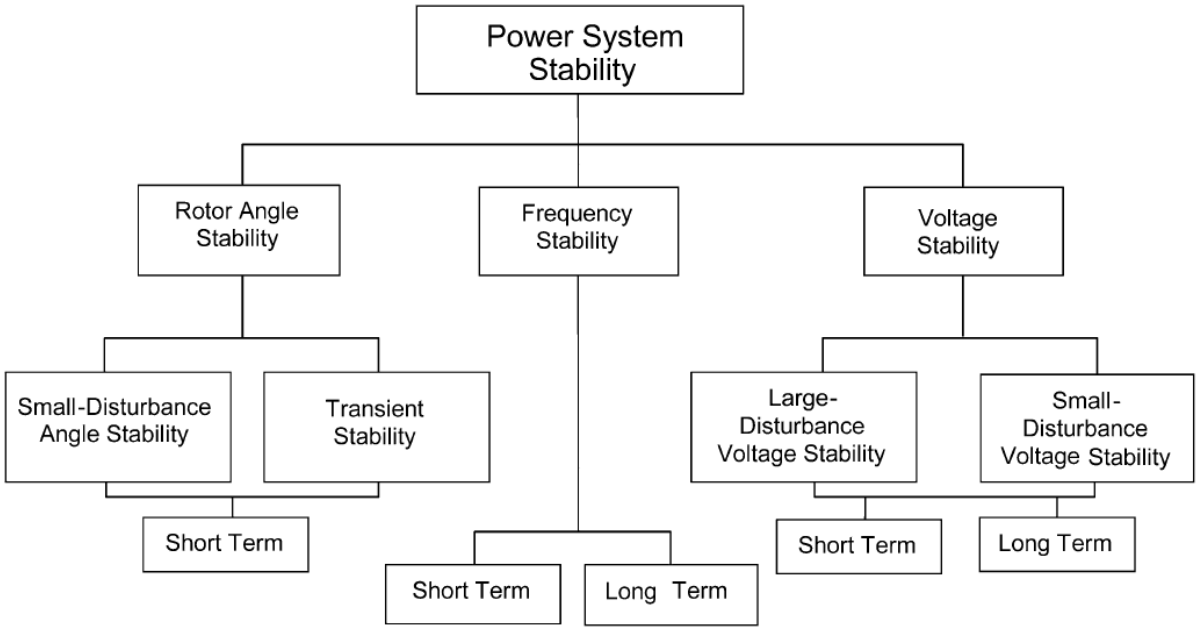

Figure 1:Classification of Power System Stability [19]

2.1.1 Voltage Stability

Voltage stability is the power system's ability to maintain acceptable voltage levels at all buses after a disturbance[19]. When a system is subjected to disturbances, fluctuations in the system conditions, or system loading that lead to an uncontrollable drop in voltage, it is said to be in a state of voltage instability. The voltage drop is directly associated with the power transfer through the transmission network's inductive reactance and loads. The system faces voltage instability if the bus voltage (V) gradually decreases even when the injection of reactive power (Q) on the same bus increases.

In the simplest form, voltage instability can be explained considering a two-terminal network as follows[1]. In the following Figure, E_S represents the constant voltage source, Z_{LN} and Z_{LD} are line impedance and load impedance and V_R is the receiving end voltage.

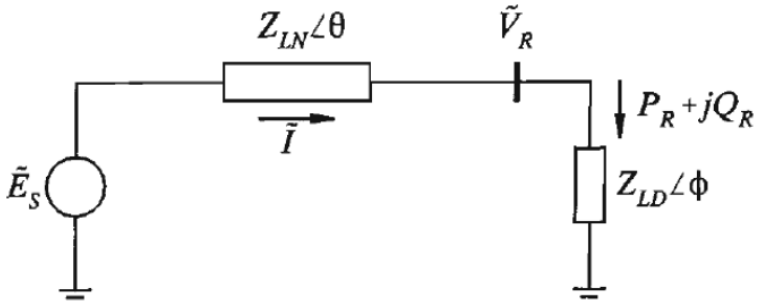

Figure 2: Simplified AC System [1]

For the system above, the following Figure shows the ratio of receiving end voltage to source voltage, line current to short-circuit current, and load power to maximum load power plotted against the ratio of line impedance to load impedance. All values are normalized to make them applicable across all transmission line impedances. When the receiving end voltage decreases faster than the current ratio can increase, the power delivered to the load increases as the voltage is driven beyond the critical value.

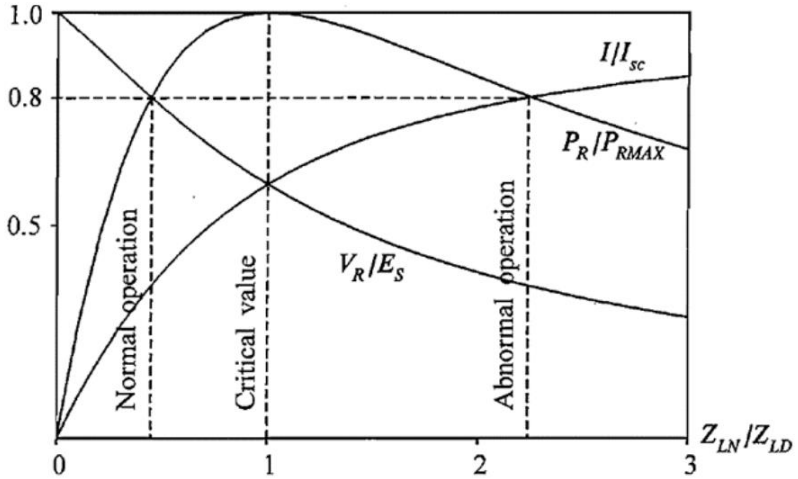

Figure 3: Ratio of a bus to source voltage compared to ratios of power, current, and loads [1]

The following plot between power versus receiving end voltage shows that as more reactive power is injected into the bus, higher voltage profiles can be obtained to supply loads showing a positive correlation between receiving end voltage and power. But in

the case of a negative relation, increasing reactive power injection leads to a rapid decrease in bus voltage, resulting in voltage instability.

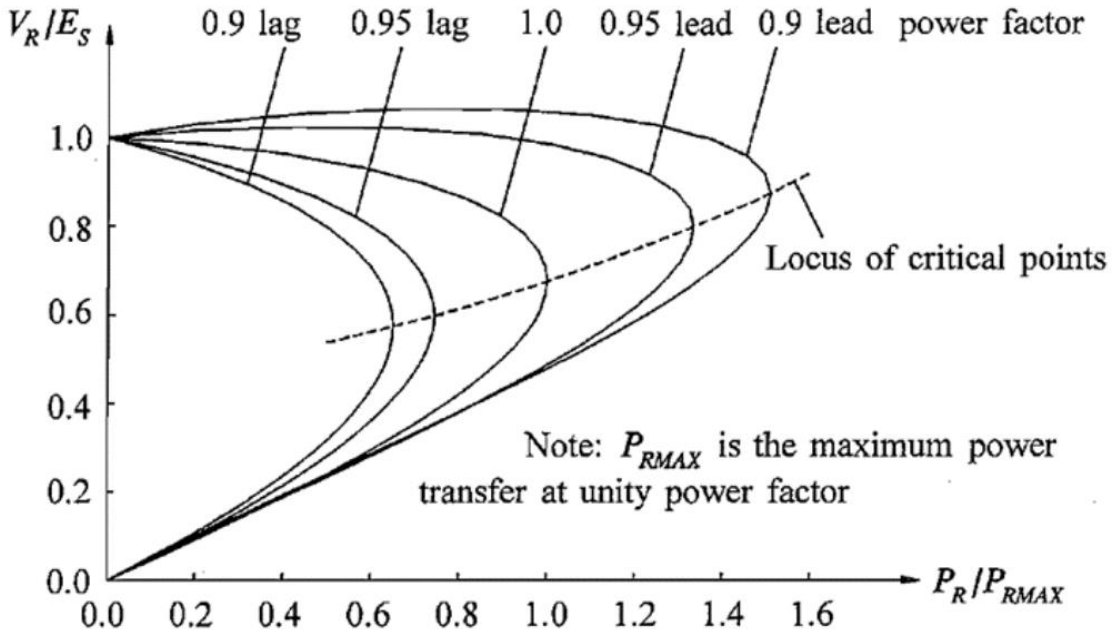

Figure 4: Ratio of a source to bus voltage vs. power plot [1]

In general, the voltage stability is mainly due to the gradual decline of bus voltages, but there can be a risk of overvoltage instability as well in some cases[20]. Similar to rotor angle stability, voltage stability is further classified based on the system's ability to hold steady voltages despite small-disturbances like load switching and large-disturbances such as system faults, circuit contingencies, and loss of generation.

2.1.2 Frequency Stability

Frequency stability is a power system's ability to return to an acceptable frequency range after a disturbance causing a significant imbalance between generation and supply clears within a specified time. Based on the operating frequency of 60Hz in the United States or 50 Hz in Europe and parts of Asia, maintaining the operating frequency within a pre-defined range around the standard operating frequency determines the frequency stability.

The deviation of operating frequency above or below the nominal indicates generation greater than load demand or load demand greater than an available generation. The conventional power system being dominantly comprised of synchronous generators with a large amount of stored energy in the form of inertia of their rotating mass made the grid resilient to large frequency deviations. As the grid is transitioning more towards

renewables and alternate sources comprising of non-conventional/ asynchronous generation, there is a need for advanced power electronics to maintain the frequency stability.

2.1.3 Rotor Angle Stability

The rotor angle stability is the capability of interconnected synchronous machines in the system to remain in synchronism[1].

The rotor angle stability can be explained using the simplified system consisting of two-machines connected by a line impedance, Z. The power flow between the machines is dependent on the voltages on both the buses, the line impedance, and the rotor angle separation between the two machines.

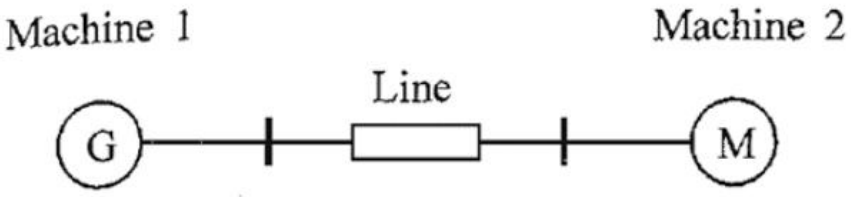

Figure 5: Two machine system connected by a transmission line [1]

The power flow is as follows:

$$P = \frac{V_1 V_2}{Z} \sin \delta \tag{1}$$

where,

P is the power from machine 1 to machine 2, V_1 and V_2 are bus voltages at bus 1 and 2, respectively; *Z* is the line impedance, and δ is the rotor angle separation.

The corresponding output power versus angle relationship shown below is a highly non-linear relationship. It can be seen that as δ increases until it reaches 90 degrees, the output power increases. Beyond this point, the output power starts decreasing. This power-angle relationship provides an essential basis to analyze the response of the machines due to system disturbances.

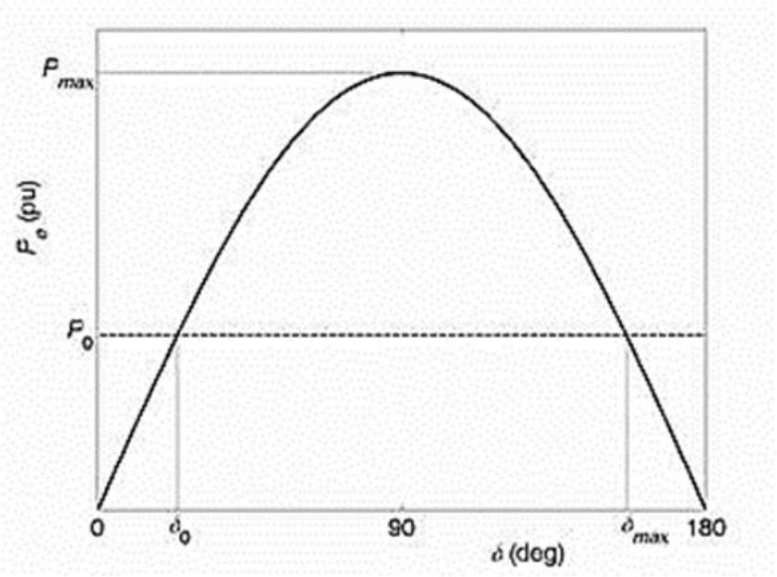

Figure 6: Output power of generator vs. rotor angle [1]

If the system's disturbance causes one of the machines to speed up, it increases the machines' angular separation. If this angular separation reaches 90 degrees, a maximum power transfer point, and then goes beyond it, the power transfer will begin to decline, causing the rotor speed to accelerate to meet the power demand, resulting in system instability.

Figure 7 depicts the rotor angle plots in one stable and two unstable cases[1]. In the first case, representing a stable condition, the rotor angle increases to a maximum due to a disturbance, decreases with oscillations damped by the system, and returns to a stable condition. In case 2, the first swing shows that the rotor angle increases, ultimately resulting in synchronism loss. Case 3 shows the situation when the system is stable initially but becomes unstable due to growing oscillations.

The rotor angle stability is further divided into small-signal and large-disturbance rotor angle stability (transient stability). Small-signal rotor angle stability deals with the power system's ability to maintain synchronism under small disturbances like load switching, while the large-disturbance rotor angle stability focuses on severe events like a short-circuit on a transmission line.

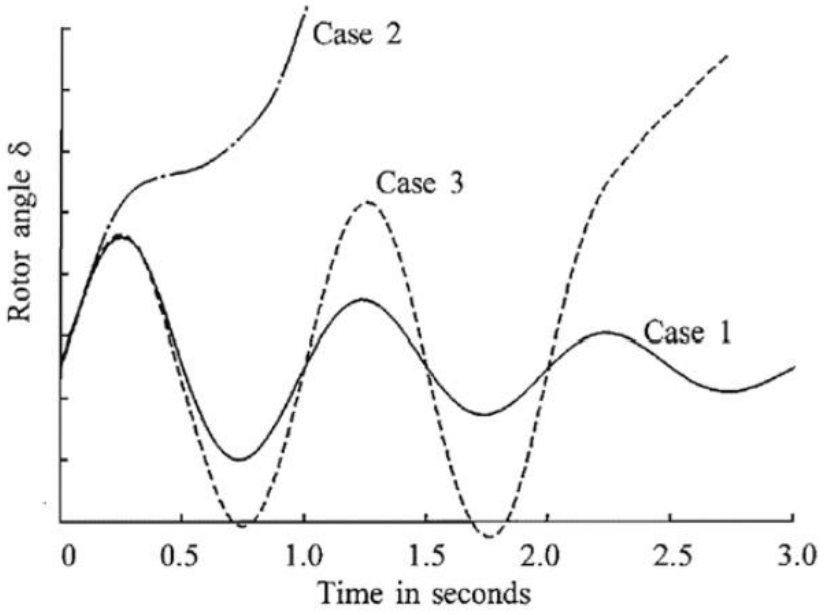

Figure 7: Different cases of rotor angle over time showing stable and unstable cases [1]

For this thesis, the focus is mainly on the system's voltage stability in cases of both large- and small-disturbances. The static voltage stability margin or steady-state voltage stability margin is discussed below.

2.2 Voltage Stability Margin- Steady State

The stability parameter calculated for the transmission line in this thesis is derived from the work presented in [15].

Let us consider a single-phase circuit element connecting two buses, m, and n, as shown in Figure 8. V_m is the voltage at the sending end and V_n is the receiving end voltage. I_n is the current flowing through the line and the Y_n is the admittance of the element. Four types of loads considered at the end of the line:

1. S_{pn} which is the constant power load
2. Y_{pn} which is the constant impedance load
3. S_{tn} is the equivalent constant power load downstream of the node n
4. SL_{tn} is the equivalent sum of all the constant power load losses downstream of the node n.

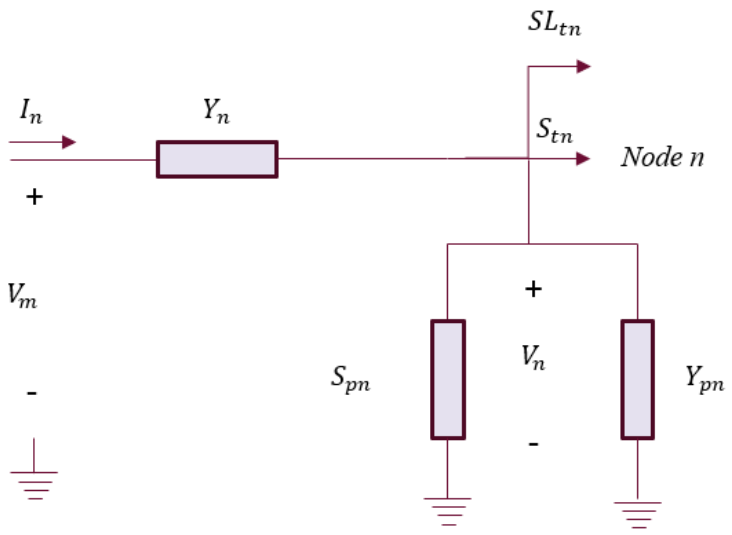

Figure 8: nth circuit element

For node n, the power flow is calculated as:

$$S_n = P_n + jQ_n = S_{pn} + S_{tn} + SL_{tn} \tag{2}$$

Receiving end power and current from element mn are:

$$V_n I_n^* = S_n + |V_n|^2 Y_{pn}^* \tag{3}$$

$$I_n = Y_n(V_{m-}V_n) \tag{4}$$

Using (4) in (3):

$$S_n = Y_n^* V_m^* V_n - (Y_{pn}^* + Y_n^*)|V_n|^2 \tag{5}$$

Separating real and imaginary part of S_n:

$$P_n = -(G_n + G_{Pn})|V_n|^2 + [|Y_n||V_m||V_n|\cos(\delta_n - \delta_m - \varphi_n)] \tag{6}$$

$$Q_n = (B_n + B_{Pn})|V_n|^2 + [|Y_n||V_m||V_n|\sin(\delta_n - \delta_m - \varphi_n)] \tag{7}$$

where,

$$Y_n = |Y_n|\angle\varphi_n$$

$$V_m = |V_m|\angle\delta_m$$

$$V_n = |V_n|\angle\delta_n$$

Using sine and cosine terms from (6) and (7), squaring and adding,

$$\alpha|V_n|^4 + \gamma|V_n|^2 + \beta = 0 \tag{8}$$

where,

$$\alpha = (G_n + G_{Pn})^2 + (B_n + B_{Pn})^2$$

$$\gamma = 2(G_n + G_{Pn})P_n - 2(B_n + B_{Pn})Q_n - |Y_n|^2|V_m|^2$$

$$\beta = {P_n}^2 + {Q_n}^2$$

Form a quadratic equation from (8), use $x = |V_n|^2$; x must be a real and positive quantity.

$$\alpha x^2 + \gamma x + \beta = 0 \tag{9}$$

The solution for x is given by:

$$x = \frac{-\gamma \pm \sqrt{\gamma^2 - 4\alpha\beta}}{2\alpha} \tag{10}$$

For x to be real,

$$\sqrt{\gamma^2 - 4\alpha\beta} \geq 0$$

or

$$\gamma^2 - 4\alpha\beta \geq 0$$

$$\gamma^2 \geq 4\alpha\beta \tag{11}$$

From (8), since x>0, α>0, β>0; it follows from (9) that:

$$\gamma \leq 0 \tag{12}$$

From (11) and (12),

$$-2(\alpha\beta)^{0.5} \leq \gamma \leq 0 \tag{13}$$

The least value of $\gamma^2 - 4\alpha\beta$ is 0. This occurs at a critical loading condition beyond which the solution does not exist. Let us define this parameter as zeta (ζ):

$$\zeta = \gamma^2 - 4\alpha\beta \tag{14}$$

When there is no loading, i.e. $S_n = P_n + jQ_n = 0$

$$\zeta_o = (\gamma^2 - 4\alpha\beta)_o = [\{2(G_n + G_{Pn})P_n - 2(B_n + B_{Pn})Q_n - |Y_n|^2|V_m|^2\}^2] + 4\{(G_n + G_{Pn})^2 + (B_n + B_{Pn})^2\}(P_n{}^2 + Q_n{}^2)$$

$$\zeta_o = |Y_n|^4|V_m|^4 \quad (15)$$

The least value of ζ =0 when $\gamma_{min} = -2(\alpha\beta)^{0.5}$

The maximum value of $\zeta = |Y_n|^4|V_m|^4$ denoted by ζ_m.

$$\zeta_m = |Y_n|^4|V_m|^4 \quad (16)$$

$$\zeta_{p.u.} = \frac{\zeta}{\zeta_m} \text{ (max=1)}$$

$$0 \leq \zeta \leq 1 \quad (17)$$

We will use ζ as the voltage stability index parameter. The parameter ζ has been referred to as a voltage stability index in the title of the thesis. The parameter ζ does not make the simplifying assumption used by the Fast Voltage Stability Index (FSVI)[20], where angles are dropped using the assumption that they are small for a balanced system. This index ζ enables the system study with imbalances as well.

3 Simulation Setup and Case Studies

3.1 IEEE 14 bus system modeled in DEW

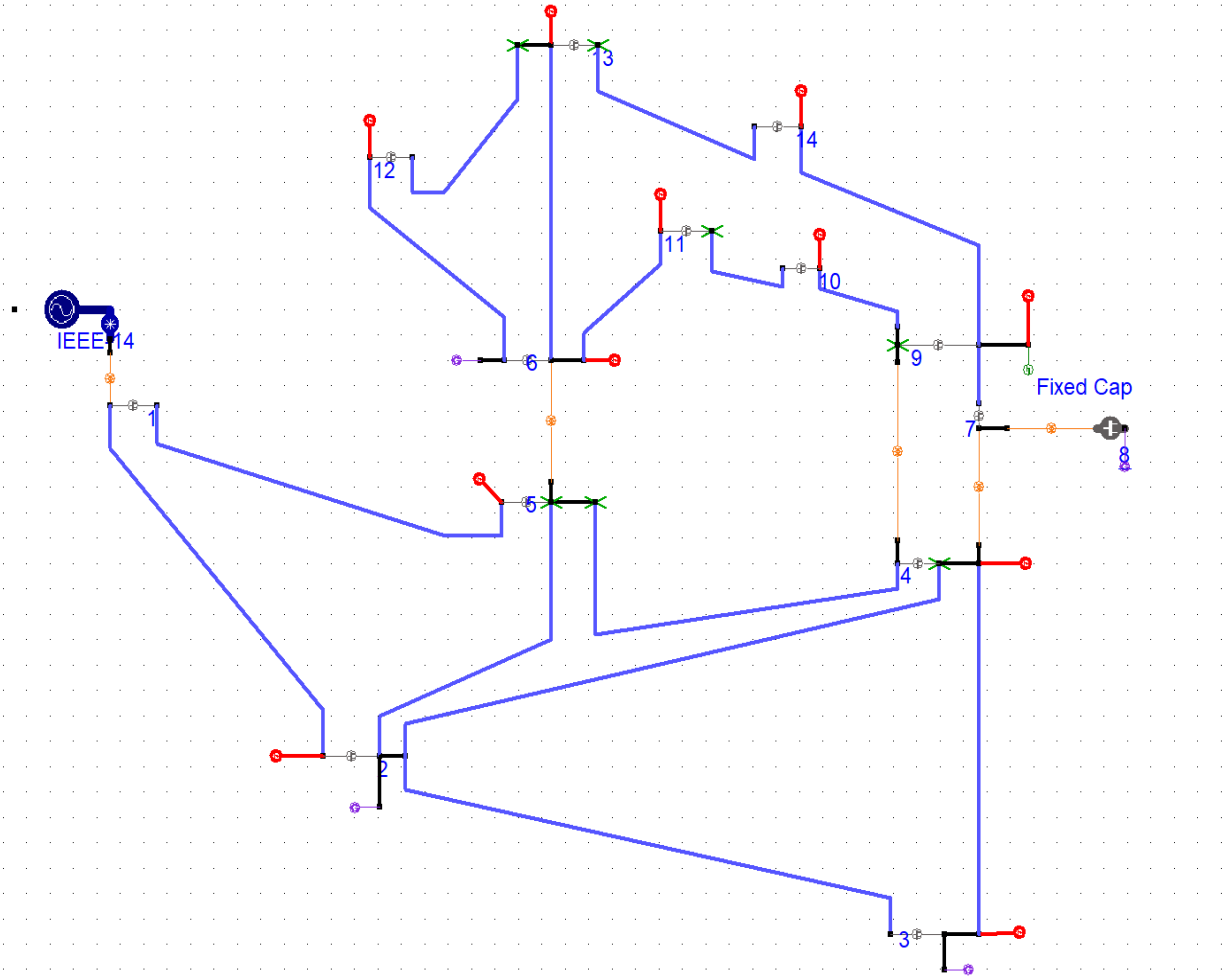

Figure 9: IEEE 14 Bus modeled in DEW

Figure 9 shows the IEEE 14 bus system. It consists of 2 generators placed at bus 01 and bus 02, and 3 synchronous compensators located on bus 03, bus 06, and bus 08. There are 11 load buses, 4 of which are fed directly through 69 kV transmission voltage, and the rest are provided by 13.8 kV.

3.1.1 Initial setup

In this experiment, the first task is to identify the weak spot in the system. For this purpose, the load is set up as a constant current model, which provides a load whose power varies with voltage as in the real world. The power factor of the load is also maintained for load variability studies, as discussed in [10]. The simulation in this part is done in two steps: Calculating the stability margin at each bus under normal loading conditions and using critical load information at each bus to generate a voltage stability matrix as a function of each bus.

3.1.2 Baseload stability margin at the individual bus level

In this step, an individual load bus is taken into consideration. The load on the selected bus is repeatedly increased by a fixed parameter ($\lambda = 1.1$), keeping all other buses at their initial loading condition. The load flow analysis is performed as long as the power flow converges after which the solution for voltage results in an imaginary number, as discussed in section 2.2.

After the process is completed at all buses, the corresponding load demand at the bus that results in the maximum power flow leading to critical loading limit, also referred to as the tip of the nose curve, is noted. Figures 10 and 11 present selected plots for the step carried out in this section. All the corresponding maximum power points are listed in Table 1 below.

Table 1: Maximum Load demand and Critical Load flow at each load bus for varying loadability limit

	Base Load		Max Load Demand		Max Power Flow		Loadability
Load Bus	P0	Q0	Pmax	Qmax	Pcr	Qcr	λ
Ld02	0.217	0.127	3.037986	1.777986	2.790438	0.544369	13.99994
Ld03	0.942	0.19	1.57	0.316665	1.735465	1.770413	1.666667
Ld04	0.478	-0.039	1.911996	0.13	1.243522	0.083638	3.999992
Ld05	0.076	0.016	2.02664	0.42664	1.212656	0.255283	26.66632
Ld06	0.112	0.075	0.671994	0.45	0.394305	0.264045	5.999946
Ld09	0.295	0.166	0.688331	0.387331	0.453481	0.254878	2.333325
Ld10	0.09	0.058	0.57	0.367327	0.326919	0.210624	6.333333
Ld11	0.035	0.018	0.525015	0.27	0.312558	0.160554	15.00043
Ld12	0.061	0.016	0.487992	0.127992	0.296205	0.07769	7.999869
Ld13	0.135	0.058	0.585	0.251329	0.344626	0.148059	4.333333
Ld14	0.149	0.05	0.49667	0.16667	0.302201	0.101411	3.333356

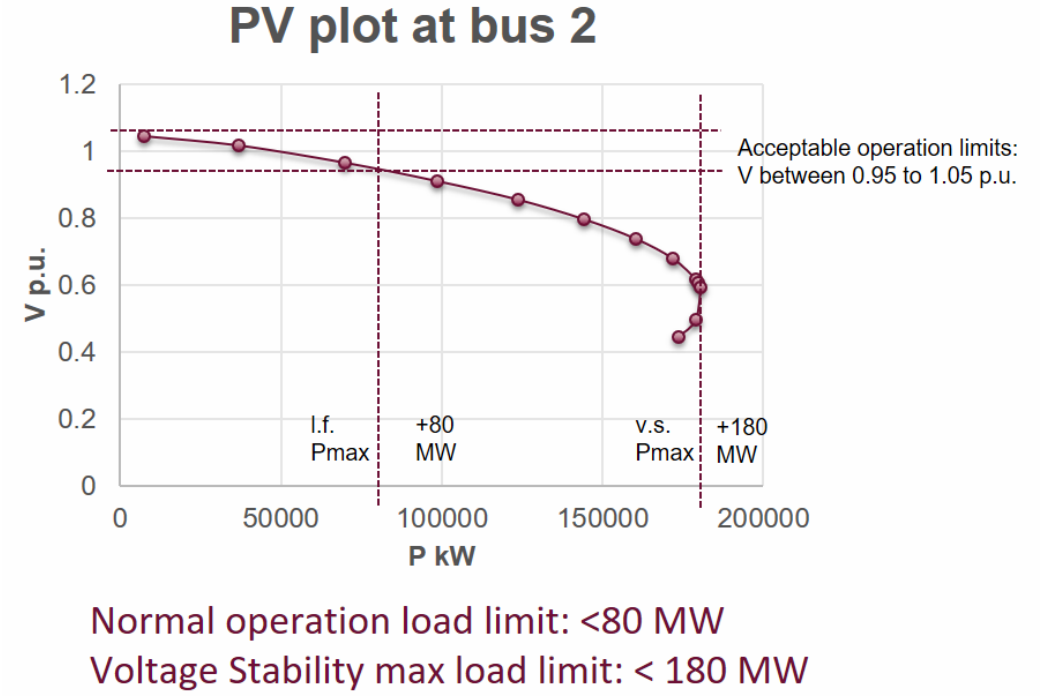

Figure 10: PV plot at bus 02

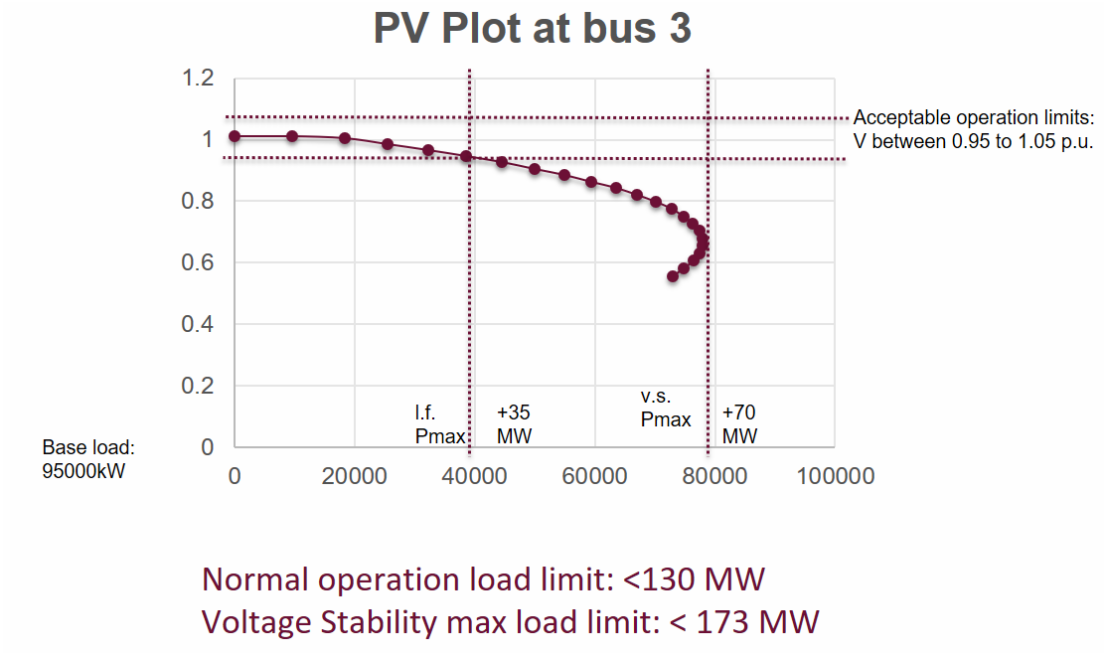

Figure 11: PV plot at bus 03

3.1.3 System-wide power flow at critical loading point

Once the steps mentioned in section 3.1.2 are completed for all the buses in the system, the process is repeated individually, setting load at the respective bus at the critical load margin found above and calculating the stability margin at all the lines. The result thus obtained is mapped for load bus against each transmission line in the system. The process is repeated for all buses and arranged in a table to produce a heat map based on the stability margin. This information is presented in Table 2. The buses are arranged according to loadability factor (increasing from left to right), and the lines are arranged on the order of average stability margin against all buses (increasing from top to bottom).

Table 2: Stability Heat Map

Loadability	1.67	2.33	3.33	4.00	4.33	6.00	6.33	8.00	14.00	15.00	26.67
Line\Bus	Bus 3	Bus 9	Bus 14	Bus4	Bus13	Bus6	Bus10	Bus12	Bus2	Bus11	Bus5
Ln 09-14	43.03	22.75	8.41	22.50	21.57	18.40	24.10	42.41	61.13	33.31	17.13
Ln 13-14	49.51	35.94	33.05	27.11	10.73	11.78	33.99	32.64	61.97	34.72	18.33
Ln 06-13	49.53	37.20	39.02	27.23	9.80	12.36	34.49	32.65	61.98	34.67	18.29
Ln 12-13	49.66	37.52	39.90	27.36	11.52	12.36	34.69	29.65	62.10	34.72	18.33
Ln 06-12	51.33	41.16	47.87	28.63	19.11	11.48	37.17	9.05	63.05	35.24	18.69
Ln 01-05	26.49	41.60	56.91	2.74	45.49	32.54	44.24	54.27	11.09	47.55	1.97
Ln 05-06	53.54	39.16	49.61	29.19	17.93	1.79	33.52	31.32	64.41	27.20	19.79
Ln 06-11	49.22	29.64	51.76	26.49	35.06	17.40	19.33	50.05	65.95	9.24	19.53
Ln 10-11	49.30	29.90	51.84	26.57	35.00	17.35	19.70	49.98	65.99	10.85	19.53
Ln 09-10	45.29	21.00	47.64	23.58	41.40	26.72	9.75	57.76	67.32	26.77	19.36
Ln 02-04	30.04	43.08	61.60	6.24	53.79	42.04	46.68	63.21	41.75	53.50	8.48
Ln 03-04	20.61	47.26	65.31	16.22	57.62	45.89	50.42	67.04	37.29	57.27	15.84
Ln 02-05	41.09	51.20	66.01	17.47	54.77	41.69	53.19	63.69	39.91	56.67	3.81
Ln 04-05	43.31	55.23	70.00	22.57	59.09	46.19	57.14	67.98	42.67	60.82	12.52
Ln 02-03	0.00	57.02	71.54	19.67	65.07	55.43	59.96	72.38	69.08	65.09	20.71
Ln 07-08	58.70	38.35	72.15	33.50	68.28	52.84	43.15	86.11	100.00	61.63	30.30
Ln 01-02	48.98	82.92	93.89	40.90	88.15	80.16	85.40	93.63	0.66	88.69	36.57

Index
100
90
80
70
60
50
40
30
20
10
0

Table 2 is useful to find the weakest link in the system. The deepest red spots observed in the table can be identified as the weak lines (row) due to the loading on the corresponding bus (column). For example, Bus 03, at the maximum loading condition, has an effect on the line ln 02-03. The system is at a critical state at this loading level of bus 03. Any further increase in loading on bus 03 will lead to a voltage collapse. Bus 03

and Bus 14 at critical stability margin will be considered a crucial spot in the analysis below.

3.1.4 Stability Margin Assessment in the presence of PV generation

3.1.4.1 Case 1 – Adding a PV plant on bus 03

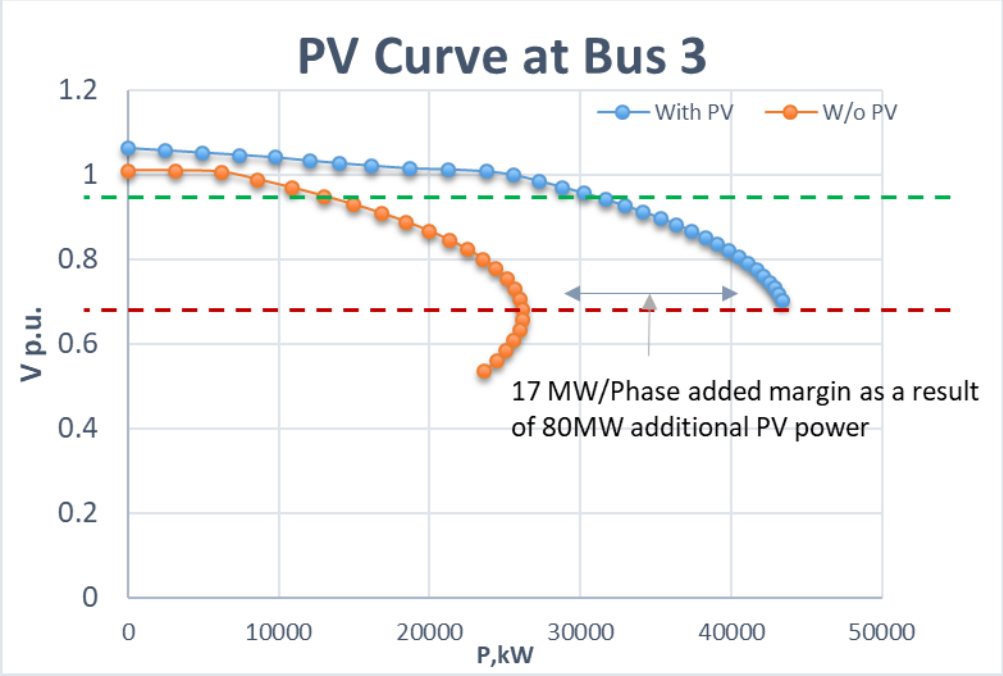

Figure 12: PV curve at bus 03 with and without PV

As indicated in the stability heat map, bus 03 is taken as a vulnerable location and studied with three PV penetration levels. Figure 12 shows the P-V curve before and after the addition of a 50 MW PV plant. The addition of the PV plant resulted in an increase in load margin by 50MW. A 25 MW and a 100 MW PV plant are added to examine if it holds the linear relationship between the amount of PV addition and rise in voltage stability margin.

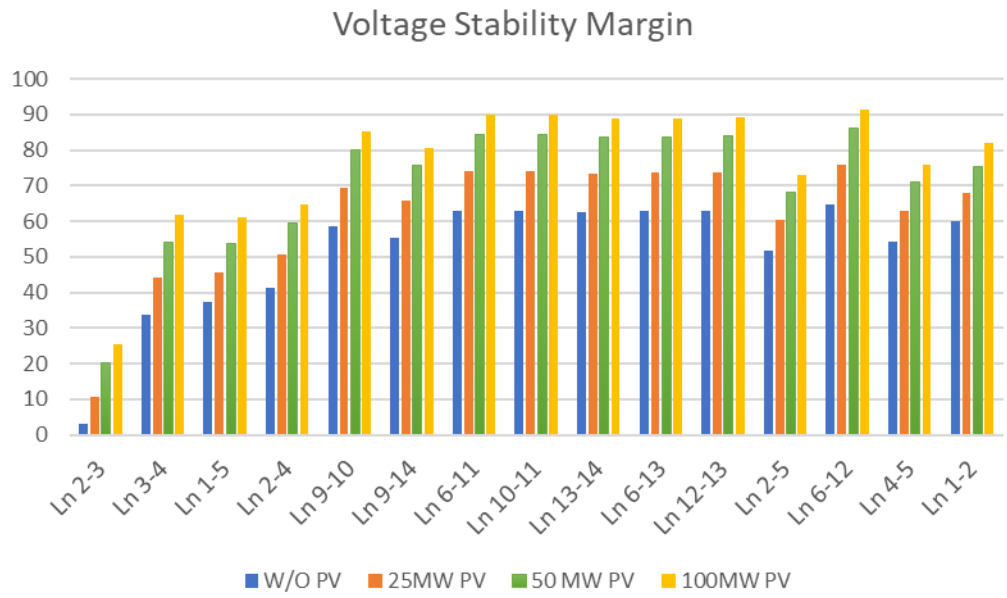

Figure 13: Voltage Stability Margin of the lines with a PV plant added on bus 03

Figure 13 shows transmission line stability margins with three levels of PV penetration on bus 03. The PV plants added are at 10%, 20%, and 40% penetration levels. For line 02-03, the stability margin rises from 10% to 20% when the penetration increases from 25 MW to 50 MW. However, an increase from 50 MW to 100 MW PV plant raises the stability margin by only 5%. Therefore, from a stability improvement standpoint, the addition of PV penetration greater than 50 MW has little effect on the voltage stability relative to bus 03. Moreover, the relation between stability margin and PV penetration level is non-linear, with a linear characteristic within a 10% to 90% stability margin region. This feature is utilized later for a separate analysis.

This case study looks at the higher voltage level of the system. As the stability heat map shows, bus 04 is the next weakest bus after bus 03. An experiment is now carried out to compare the stability margin improvement when the PV plant is added at bus 04 instead of bus 03.

In this experiment, the loading on bus 03 is maintained at a critical level, as in the earlier case. The stability margin of the lines is calculated in both the scenarios discussed. As shown in Figure 14, the addition of PV at bus 04 shows improved stability margin on all the other lines except Line 02-03. Since the loading at bus 03 is at a critical level, it is justified that adding a PV plant on bus 04 contributes to voltage improvement by a smaller margin than the one added on bus 03. Therefore, bus 03 is considered the best location in the higher voltage zone in voltage stability margin analysis.

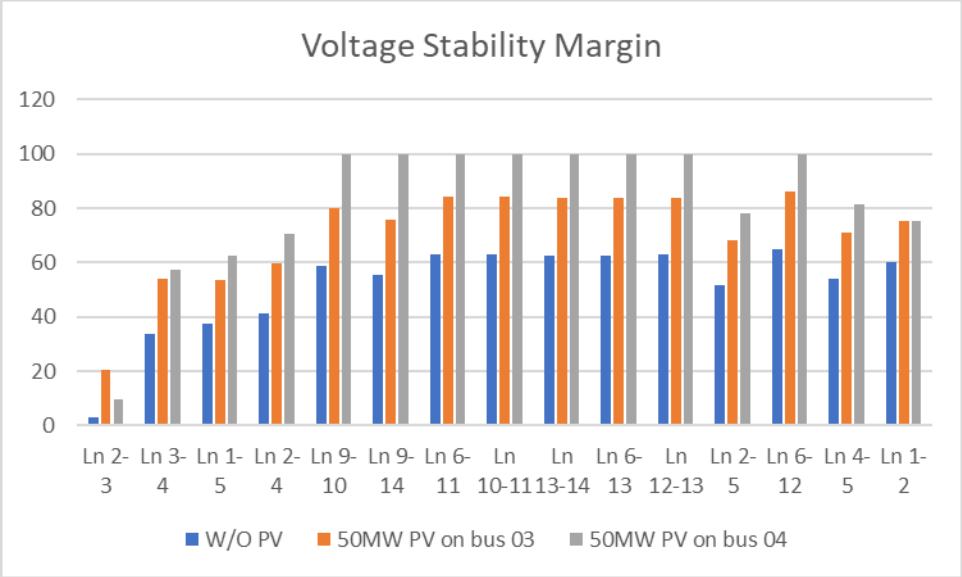

Figure 14: Voltage Stability Margin of the lines with a 50MW PV plant on bus 03 and bus 04, respectively.

3.1.4.2 Case 2 – Adding a PV plant on bus 14

Based on the stability heat map discussed in section 3.1.3, another location of interest for stability margin assessment is bus 14, which is in the system's lower voltage region. In this case, a 25 MW and a 50 MW PV plant are added on bus 14, and the calculations follow the steps as in Case 1.

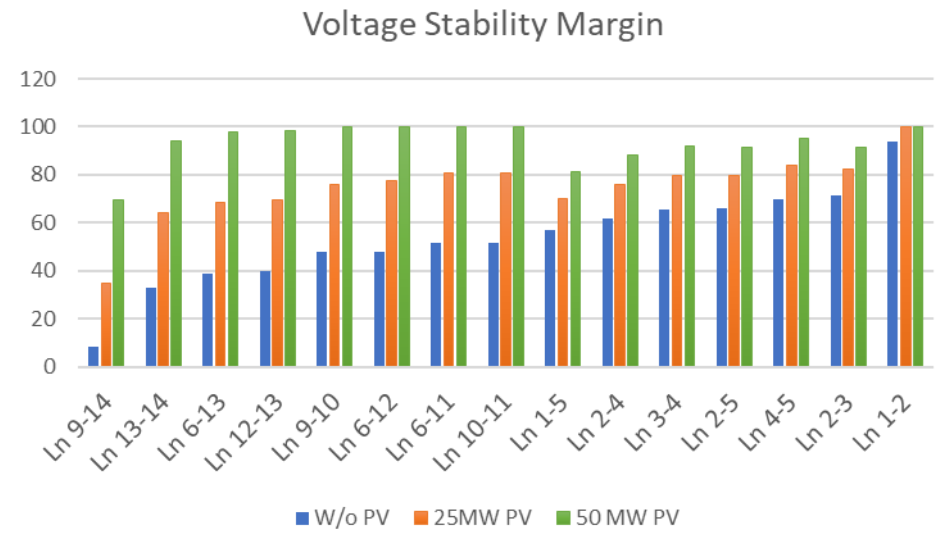

Figure 15: Voltage Stability Margin of the lines with a PV plant added on bus 14

The results obtained are presented in Figure 15. The lines are sorted in the increasing order of stability margin calculated when bus 14 is critically loaded. It is observed that the addition of a 50 MW PV plant on bus 14 improves the voltage stability margin of the lines in the lower voltage region compared to a 25 MW PV plant.

On the contrary, the stability margin increment in the higher voltage region is not significant. This situation is the indication that a higher penetration level on this bus is problematic for the system. This issue becomes apparent in the dynamic simulation performed in section 3.2.

3.1.5 Stability Margin estimation for different PV penetration levels

Both cases 1 and 2 above show the non-linear relationship between rising PV penetration level and stability margin. However, in the region of 20% - 80% stability margin, the trend is found to be linear. This linear segment can help estimate the system state when any PV plant is out of service.

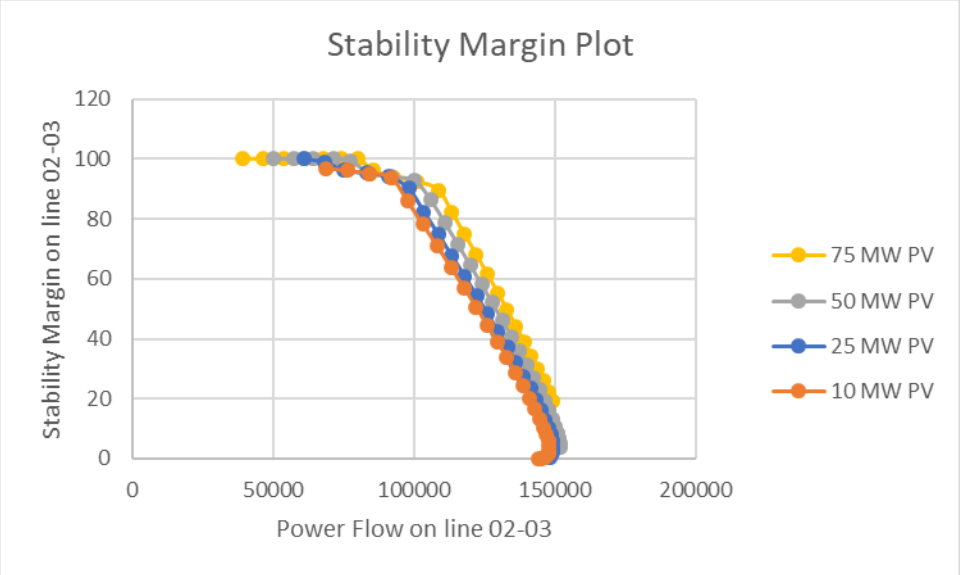

Figure 16: Stability Margin Assessment under different PV penetration levels on bus 03

For this purpose, linear regression analysis is done in the curve's linear section shown in Figure 17. A regression equation is developed to estimate the change in stability margin due to changes in line loading. The evaluations of linear regression equations, along with the goodness of fit, are presented in Table 3.

The variable used for the regression are: y = Transmission Line Loading (MW), and x = Stability Margin (%) in the 10% - 90% region. As evaluated using the standard R-Squared (R^2) metric, the goodness of fit is greater than 95% for all scenarios considered in this analysis. In the No PV scenario, the increment of 1% stability margin requires the reduction of 1.79 MW of line loading, whereas, in the case of PV addition, a similar increment in stability margin requires a drop of only about 0.65 MW of line loading. This trend does not hold beyond the 10%-90% range; however, the danger of system collapse is significant when the stability margin drops below 10 %, whereas higher than 90% is not much of a concern. Therefore, estimation in this 10%-90% range is reliable and useful for calculating MW distance to the critical point before under-frequency load shedding (UFLC) activates.

Table 3: Formation of the regression equations for line 02-03 under different PV penetration scenario on bus 03

Scenario	Linear regression equation for X ∈ (10,80)	Goodness of fit R^2
No PV	y = -1.7988x + 452.23	R² = 0.9539
10 MW PV	y = -0.644x + 154.04	R² = 0.9982
25 MW PV	y = -0.6254x + 155.63	R² = 0.9979
50 MW PV	y = -0.5889x + 157.88	R² = 0.9976
75 MW PV	y = -0.5785x + 161.14	R² = 0.9987

3.2 IEEE 14 bus system modeled in OpenModelica

In section 3.1, steady-state voltage stability analysis is presented, experimenting with various PV penetration levels and observing the bus voltages and line power flow. This section expands the similar scenarios to include the generator and PV inverter (DER) responses. All the system components such as generation level, line parameters, and system loading are kept similar to that used in the steady-state analysis above. However, control parameters for DER and generators vary in this case for tuning purposes. The experiment's objective in this section is to examine if the observation made in the steady-state analysis holds from different perspectives. The simulation uses Modelica language in OpenModelica software, and the process is described further in the following paragraphs.

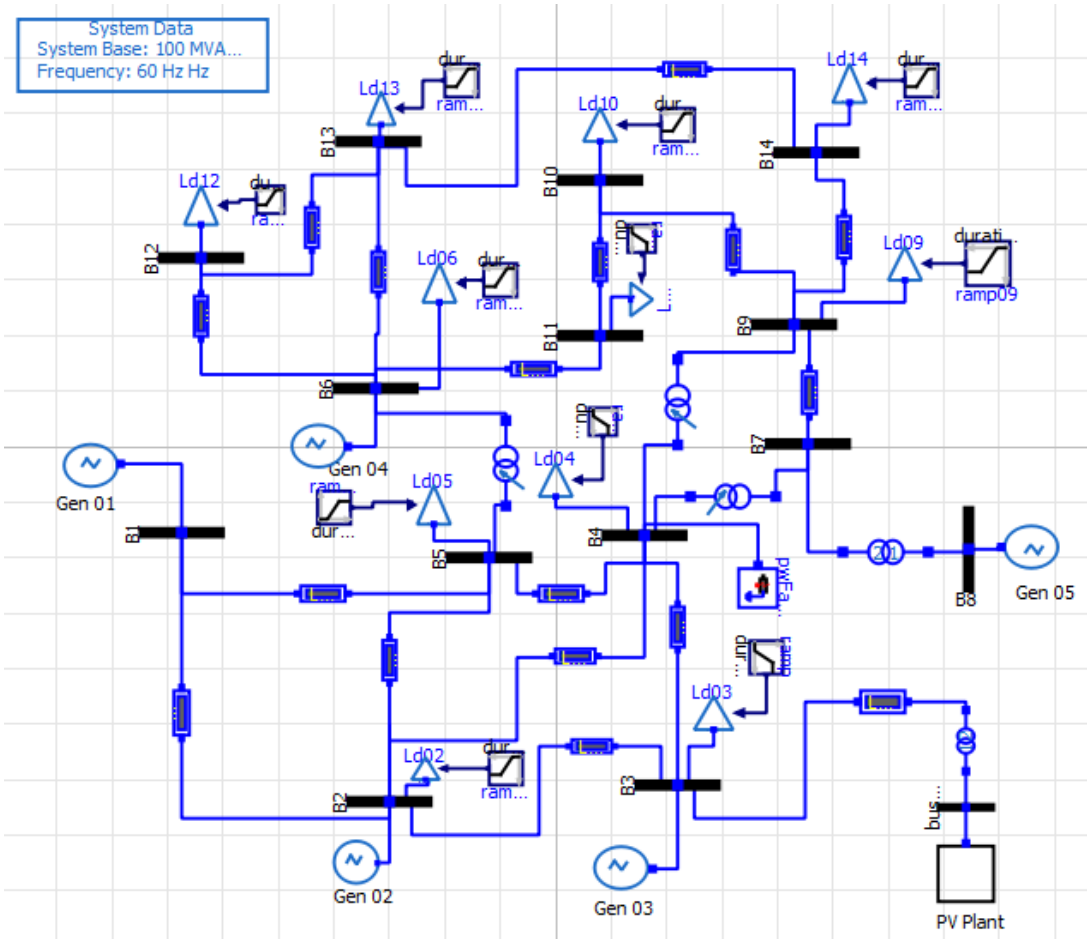

Figure 17: IEEE 14 bus modeled in OpenModelica

3.2.1 Initial Setup

A complete model developed in OpenModelica is shown in Figure 17. Gen 01 represents the start of the feeder. Loads are set to the constant current mode, initialized at baseload values, and varied using the ramp signal generator block. Since this study focuses on voltage stability, the observations are made after the system reaches a steady-state condition.

3.2.1.1 PV inverter model

The PV inverter model used in this simulation considers the ideal dc source in the input terminal. The modeling is done utilizing abc to dq conversion. The difference of desired voltage (Vref) and measured voltage (V) at a given bus is passed through a PI controller to generate reactive power reference (Qref). The module can be programmed to define reactive power injection during a closed-loop Q control on a designated bus with the addition of a dead band to prevent excessive flickering around the set points.

Using Qref(Q*), vd(Ud), and vq(Uq), reference currents idref(id*) and iqref(iq*) are generated, which is again passed through the current controller to generate the currents id and iq required for PWM signal generation. Figure 18 shows the block diagram of the inverter control.

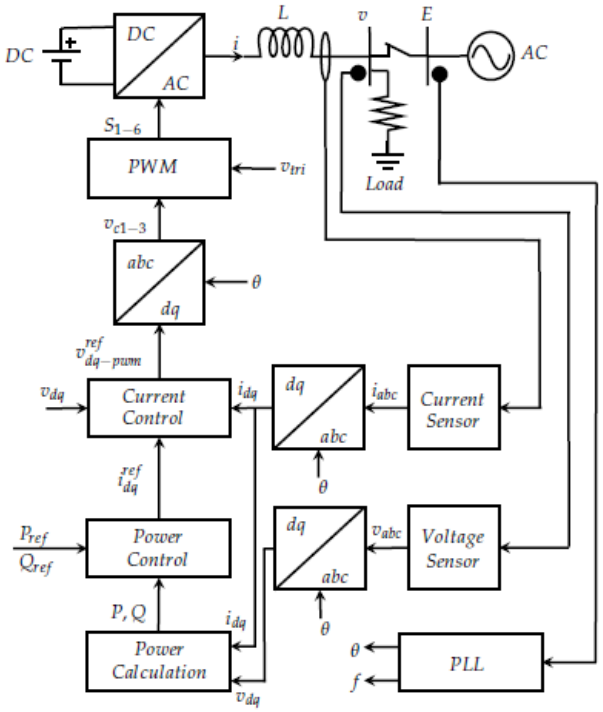

Figure 18: Inverter control used in the simulation.

Figure 19 shows the volt/VAR control scheme. This curve defines the level of VAR to be generated or absorbed by the inverter to support the grid voltage at the desired level (VN). In this Figure, the inverter generates at the rate defined by the slope of the line connecting (V2, Q2) and (V3, Q3). Similarly, absorbs in the region between (V4, Q4) and (V5, Q5). However, the region between (V3, Q3) and (V4, Q4) is a dead band, and the inverter does not change the reactive power in this region.

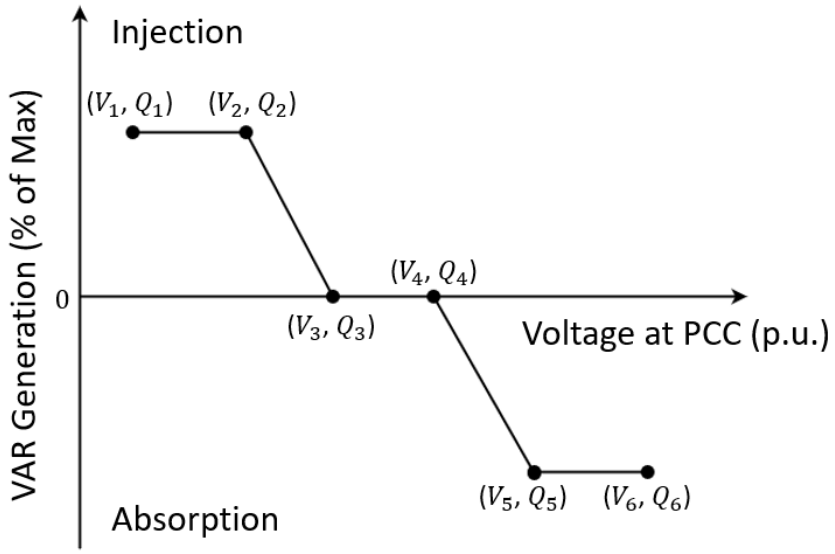

Figure 19: Volt-Var control scheme

3.2.1.2 Large-Disturbance test

The model is tested against a switched load on bus 03 after 5 seconds of operation to ensure the system behaves as expected. The system's response, notably Gen 01 against this disturbance, is observed and shown in Figure 20. The reaction at generator 1 shows the system's ability to return to the normal operating condition once the fault clears in 0.5 seconds.

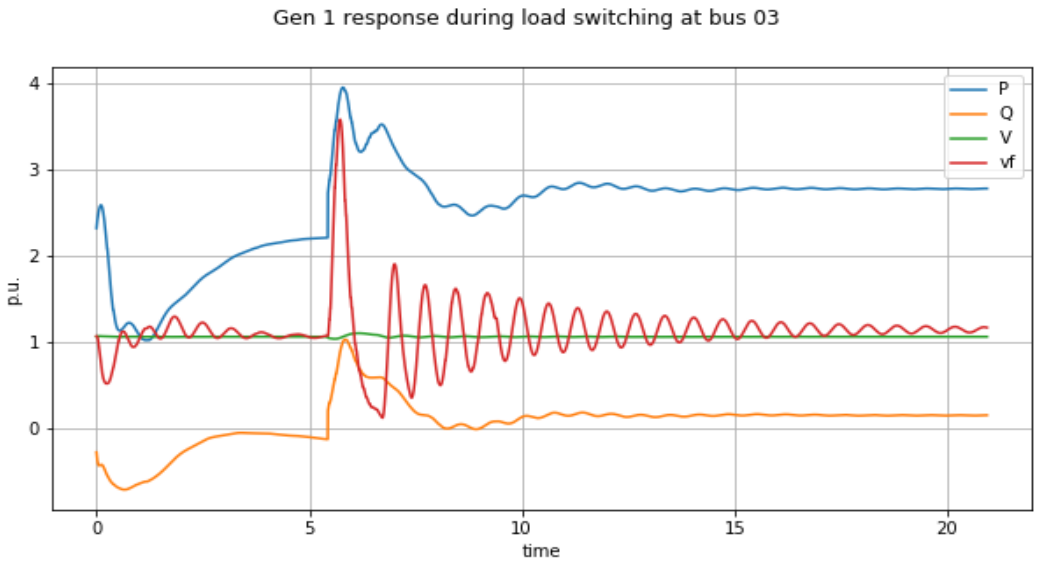

Figure 20: Reaction of Generator 01 to a step load switching from 1 p.u to 2 p.u on bus 03

Next, a three-phase fault is introduced on bus 03. After starting and operating the model for 5 seconds, the fault activates for a duration of 0.5 seconds. Once the simulation completes, terminal voltage (V), field voltage (vf), active power (P), and reactive power (Q) at the generator's terminal is shown in Figure 21. After the fault clears, all four parameters- P, Q, V, and vf return to the pre-fault level. This indicates that the system model is stable under the normal operating condition and can be used for further analysis.

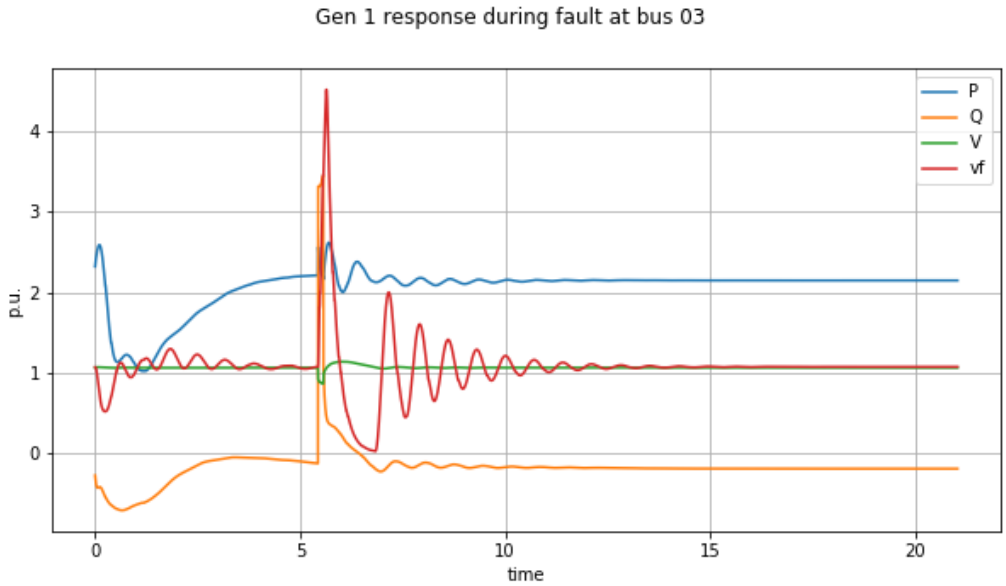

Figure 21: Generator 1 responses to a three-phase fault on bus 03

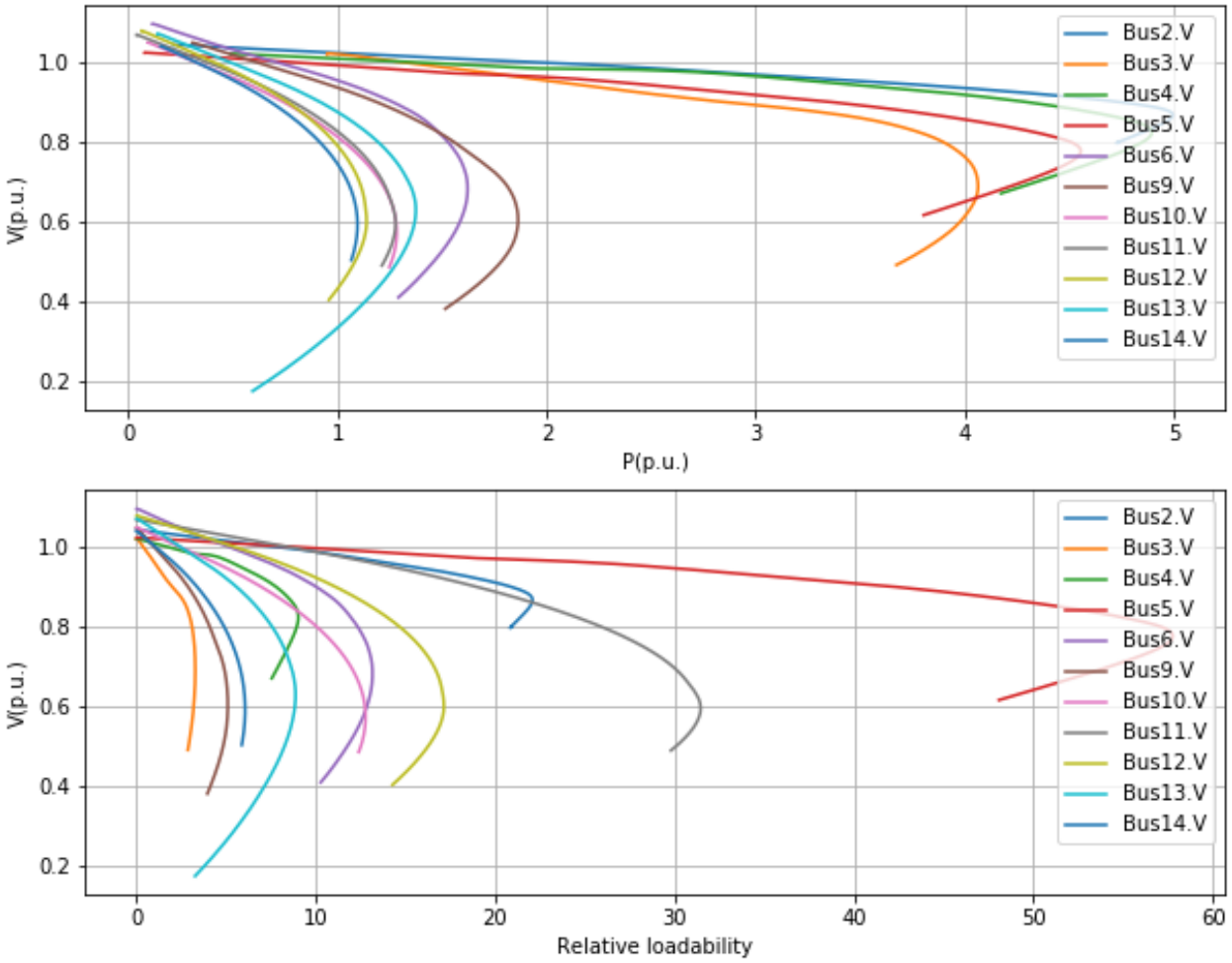

Figure 22: P-V curve plot for the IEEE -14 bus system using Open-modelica

3.2.2 Stability analysis in the presence of PV plant

3.2.2.1 Adding a PV plant on bus 03

As described in section 3.1, bus 03 is a preferred location for PV plant integration. The effect of solar irradiance and cell temperature is kept constant at 1000w/m^2 and 25 degrees centigrade. Therefore, the DC voltage remains constant at the incoming terminal of the PV inverter. The power available at the PV plant's output terminal is stepped up using a transformer and connected to the grid at bus 03 through a transmission line. The penetration level is set at 0 MW, 50 MW, and 100 MW to study the impact on voltage stability. The load on bus 03 ramps after 5 seconds at the rate of 1 p.u per second until the system collapses for each penetration level. A P-V curve is plotted for each penetration level and shown in Figure 23. A 50MW PV penetration shows the critical load margin improvement by one p.u compared to the base case.

However, doubling the PV penetration level to 100 MW increases the margin by only 1.5 p.u. This confirms the non-linearity in margin improvement under various penetration levels, as discussed in steady-state analysis in section 3.1.

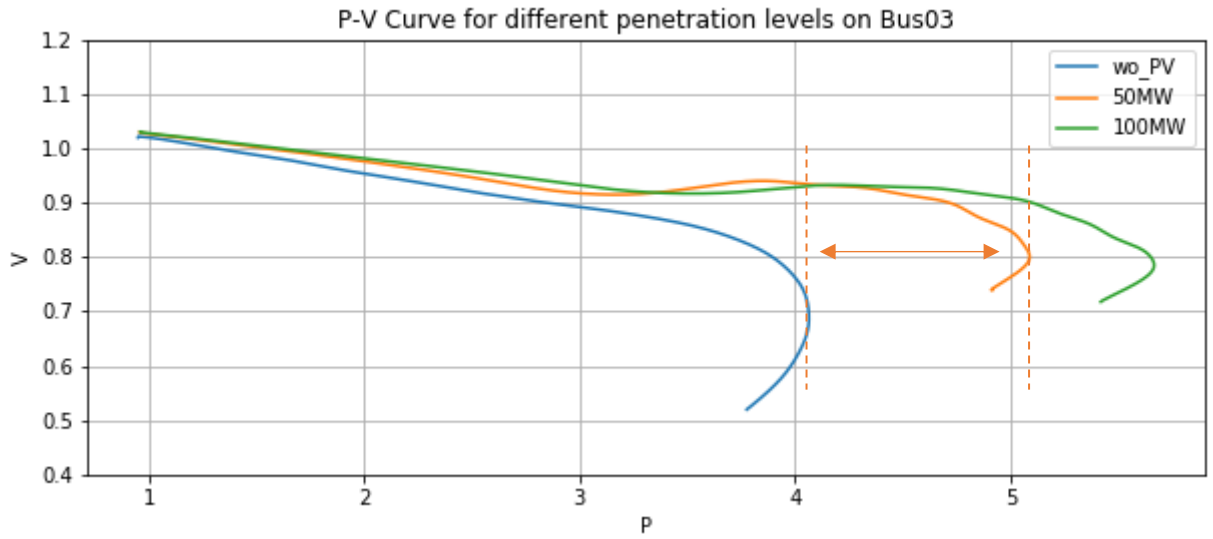

Figure 23: P-V curve at bus 03 with and without PV generation

The parameters P, Q, and V at the generator terminal, PV plant terminal, and the load bus terminal are shown in Figure 23. The column on the left represents the base case (No PV), and the right column represents the 100 MW PV penetration scenario. In the base case, there is no PV plant supplying power to meet the demand on bus 03, and therefore, the generator is the only source. As the load demand increases, the power flow first increases up to 4 p.u, but the bus voltage begins to fall. This leads to the stress in the generator's excitation system to meet the required reactive power as it tries to restore the voltage on bus 03. Eventually, the generator excitation system saturates, and the system collapses.

However, the reactive power supply from the PV inverter of 100 MW PV supports the load voltage, reducing the generator's supply. However, the active power demand keeps increasing as the load ramps up, and the generator overloads and trips eventually.

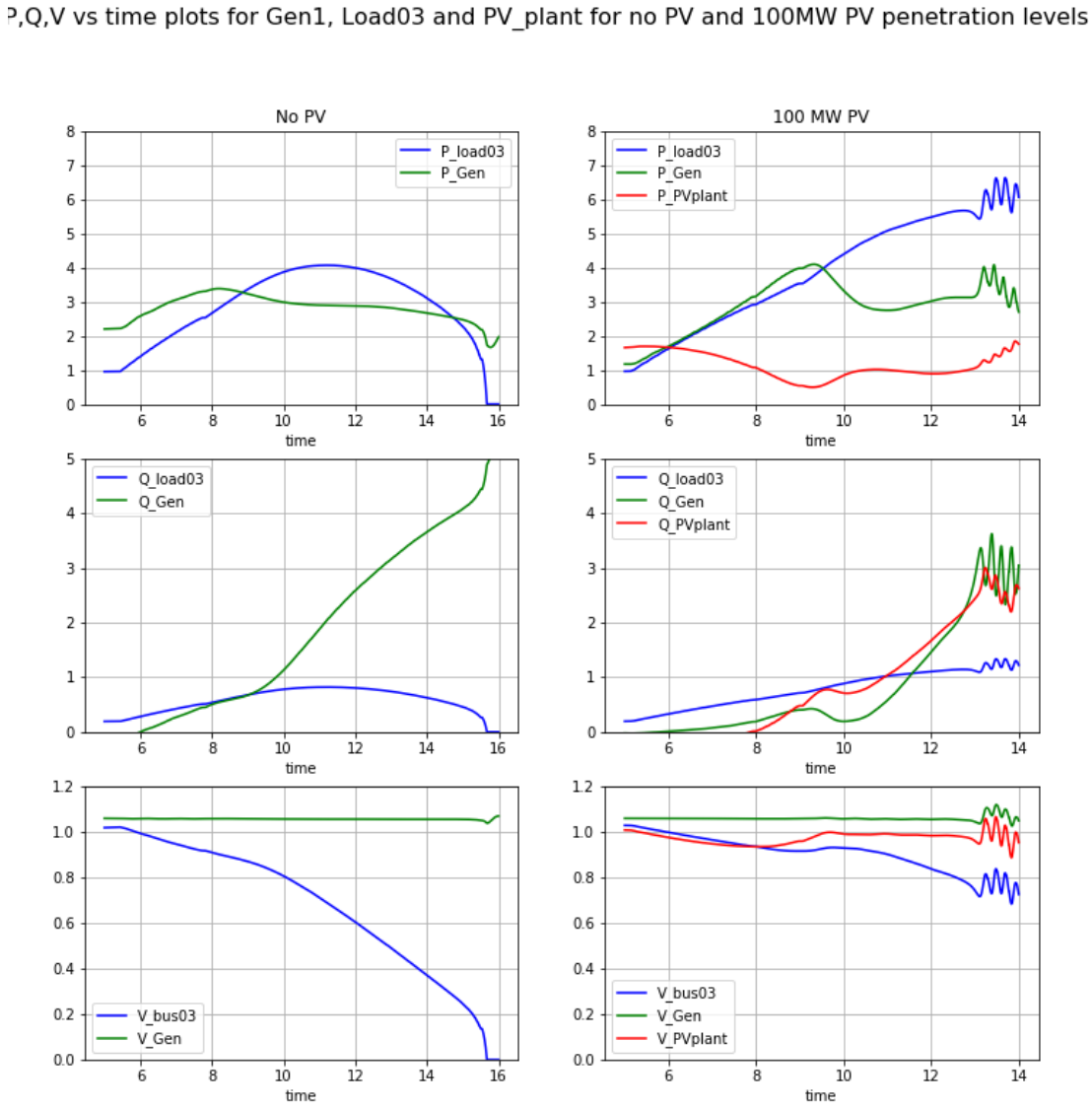

Figure 24: Comparative plots for P, Q, and V among Load bus, generator, and PV plant

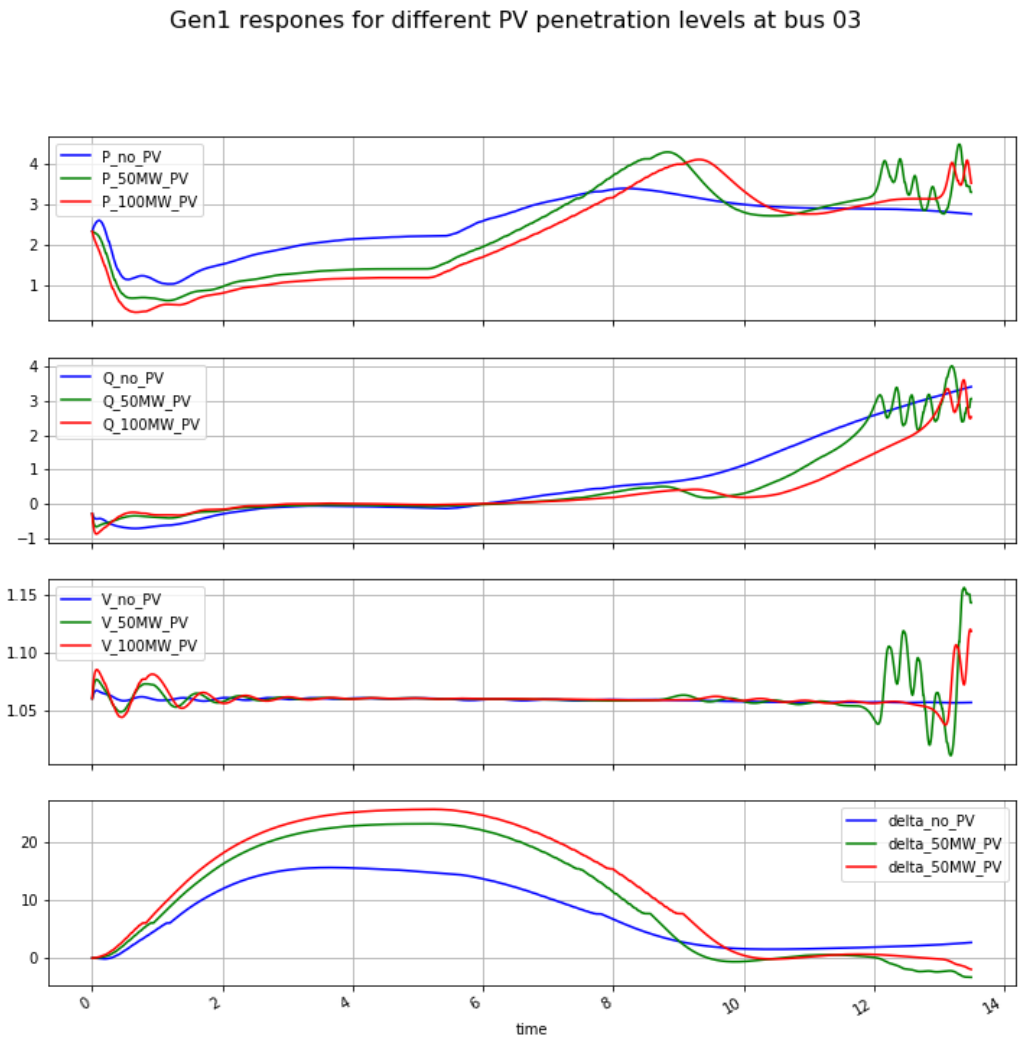

Figure 25: Generator response for base case, 50 MW PV and 100MW PV

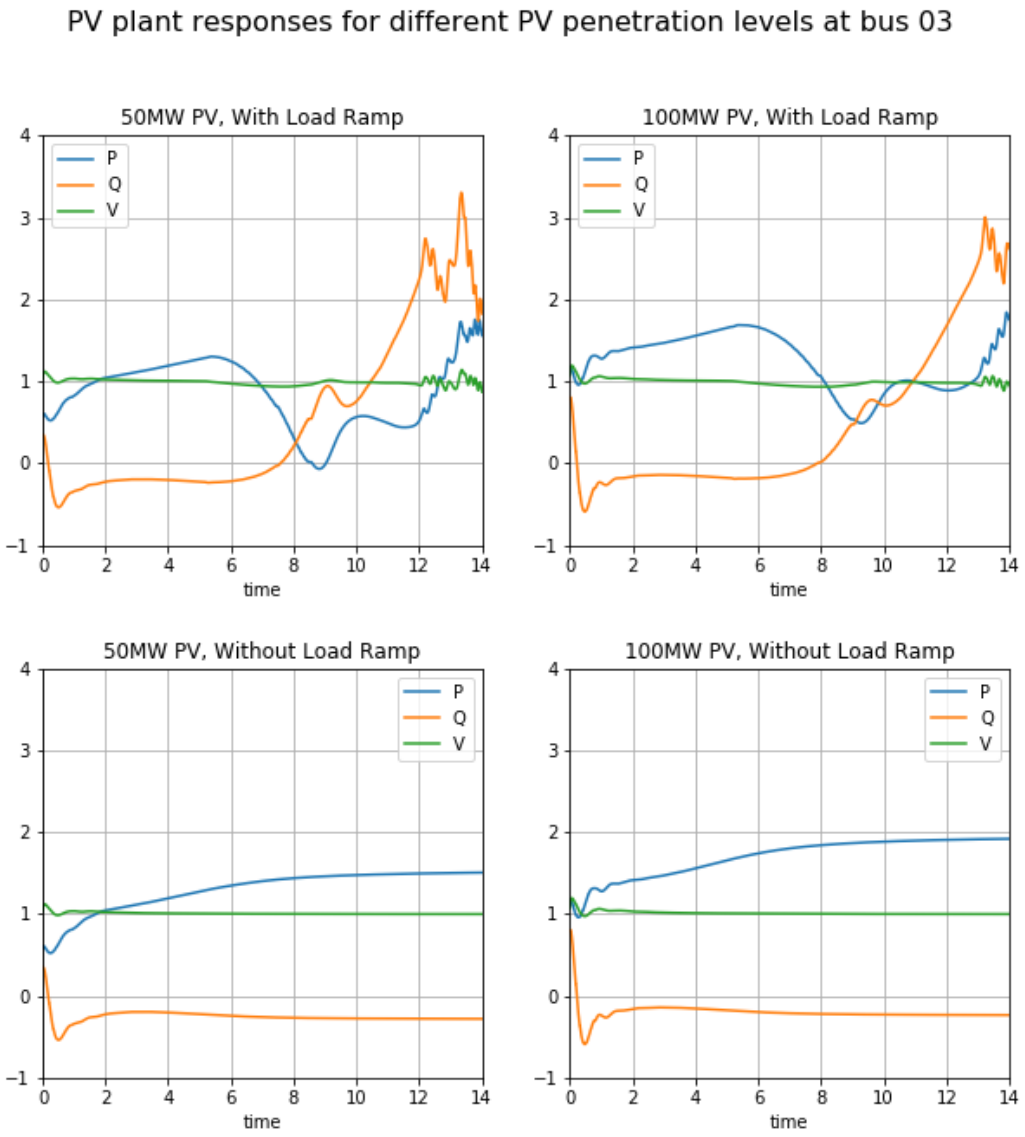

Figure 26: PV plant responses for 50 MW and 100 MW PV penetration on bus 03

3.2.2.2 Adding PV plant on bus 14

In this case, the PV plant is added on bus 14, and the parameters remain the same as the previous case. The load on bus 14 is ramped for three PV penetration levels- 0 MW, 50 MW, and 100 MW. Figure 24 presents the P-V curve for three PV penetration levels.

One noticeable difference in this case compared to the PV plant added on bus 03 is that for 50 MW PV penetration, the MW distance to instability is lesser than that of no PV penetration. This scenario becomes apparent as the responses of the generator and PV plant are studied.

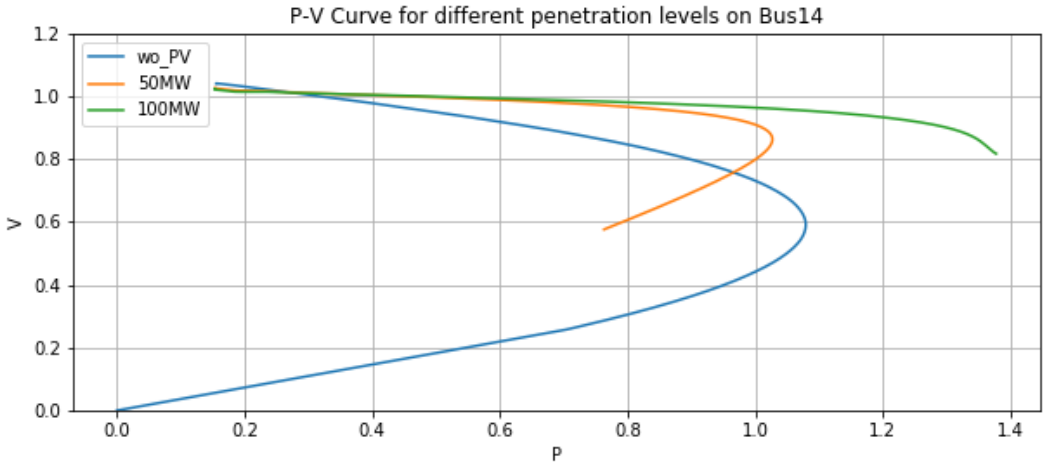

Figure 27:P-V curve for 0 MW, 50 MW, and 100 MW PV plant

In the case of 50 MW PV penetration, the required reactive power is supplied mostly by PV itself to support the voltage. As demand rises, the stress on the PV inverter increases, as shown in figures 25, 26, and 27. However, generator 01 is operating under normal conditions. The PV inverter overloads itself and causes instability in the whole system. Protection against this potential instability requires advanced control settings such as fast frequency response and inertial response.

In the case of a 100 MW PV plant, the results are similar to that of the 50 MW PV plant except for 0.4 p.u higher amount of load served.

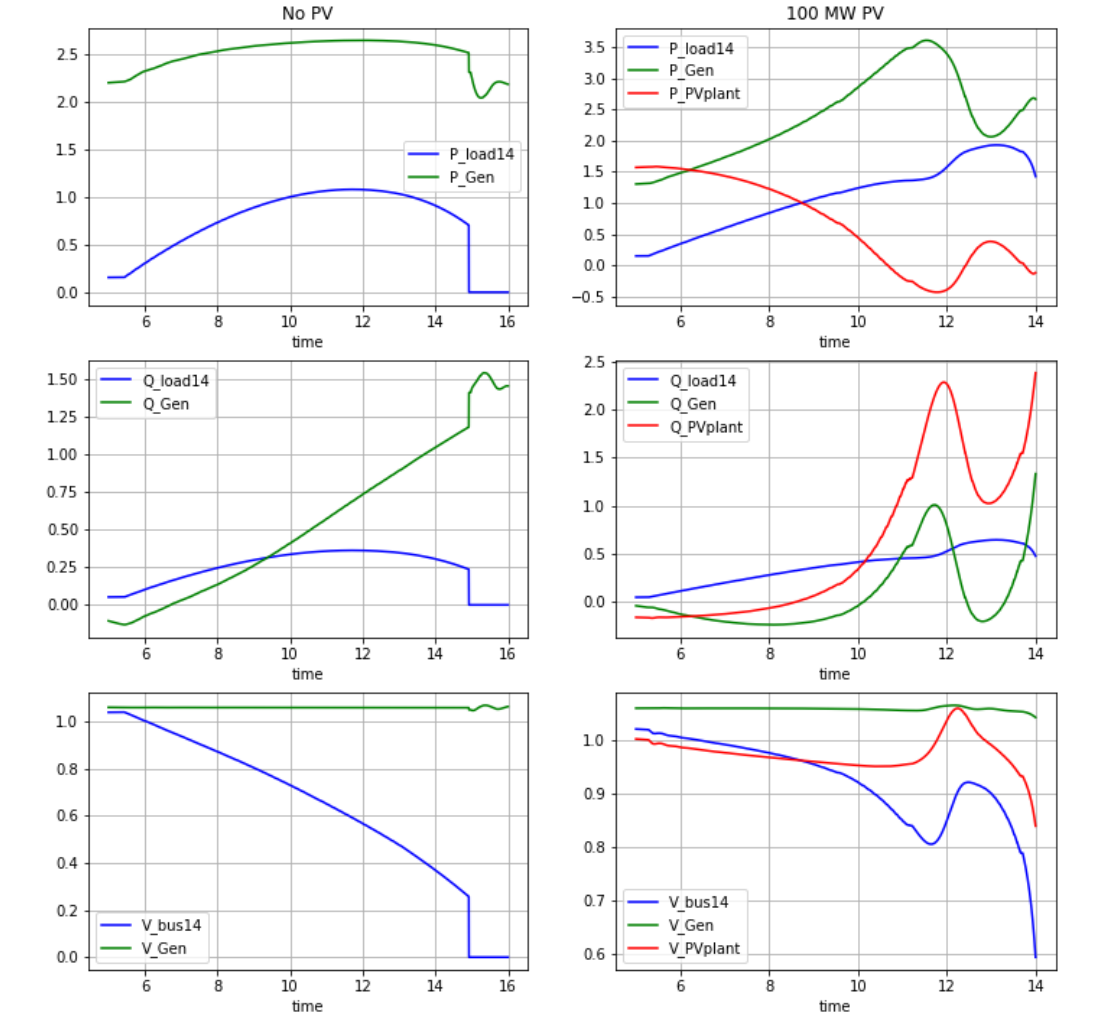

Figure 28: P, Q, and V plot for generator, PV plant, and load bus 14 for no PV and 100 MW PV

Figure 27 shows the comparative plot for 100 MV PV vs base case scenario looking at the variables P, Q, and V from generator terminal, Load and PV terminal. The case with 100 MW PV shows that the voltage on bus 14 is kept above 0.8 p.u. as the reactive power is supplied by PV at its max and rest supplied by the generator. As the voltage improves the demand also improves at the load terminal therefore, the generator active power output also increases to its maximum capacity to meet the demand. As both PV and Generator operate beyond rated capacity, the voltage on bus 14 starts to drop quickly and the system becomes unstable.

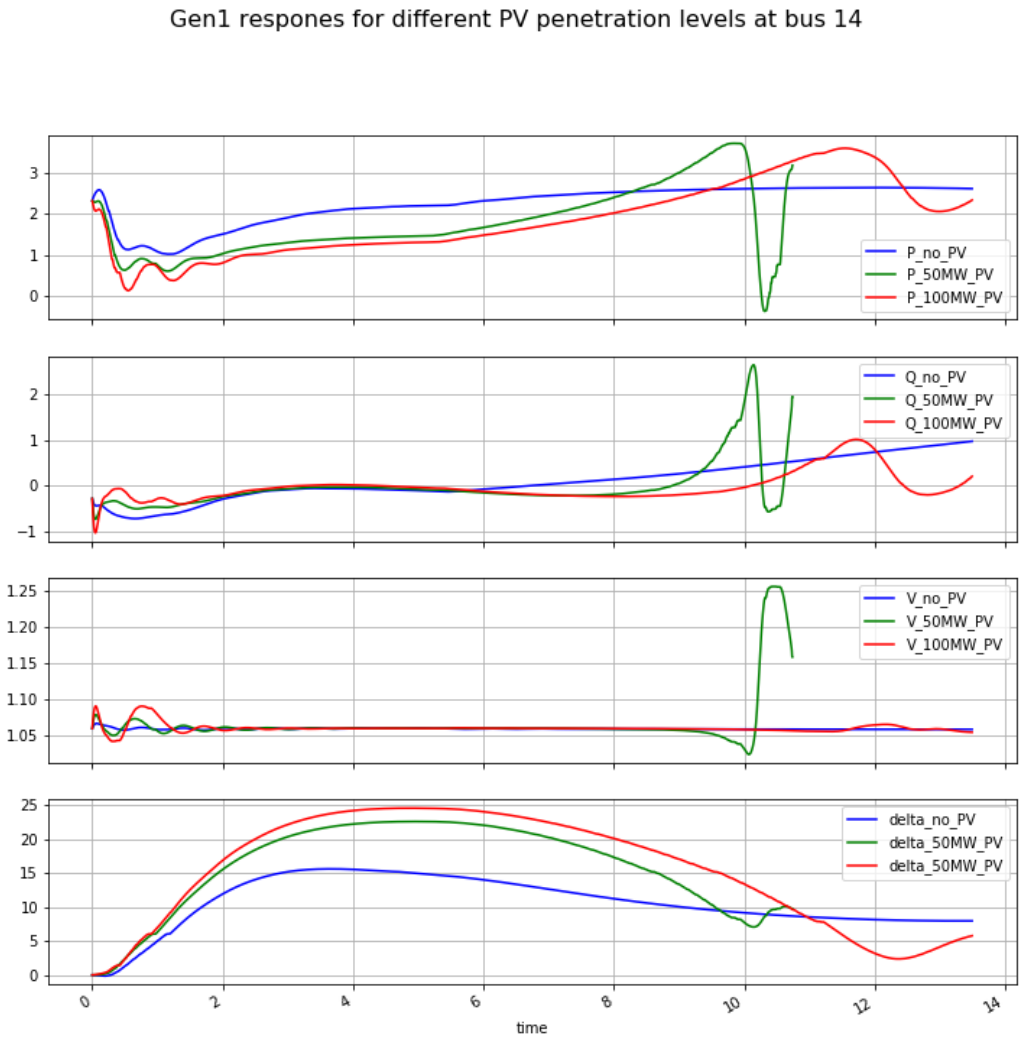

Figure 29: Gen 1 responses for different PV penetration level on bus 14

Figure 28 represents the P, Q, V, and rotor angle as recorded at the generator 1 terminal. Addition of 50 MW PV shows that the system becomes more

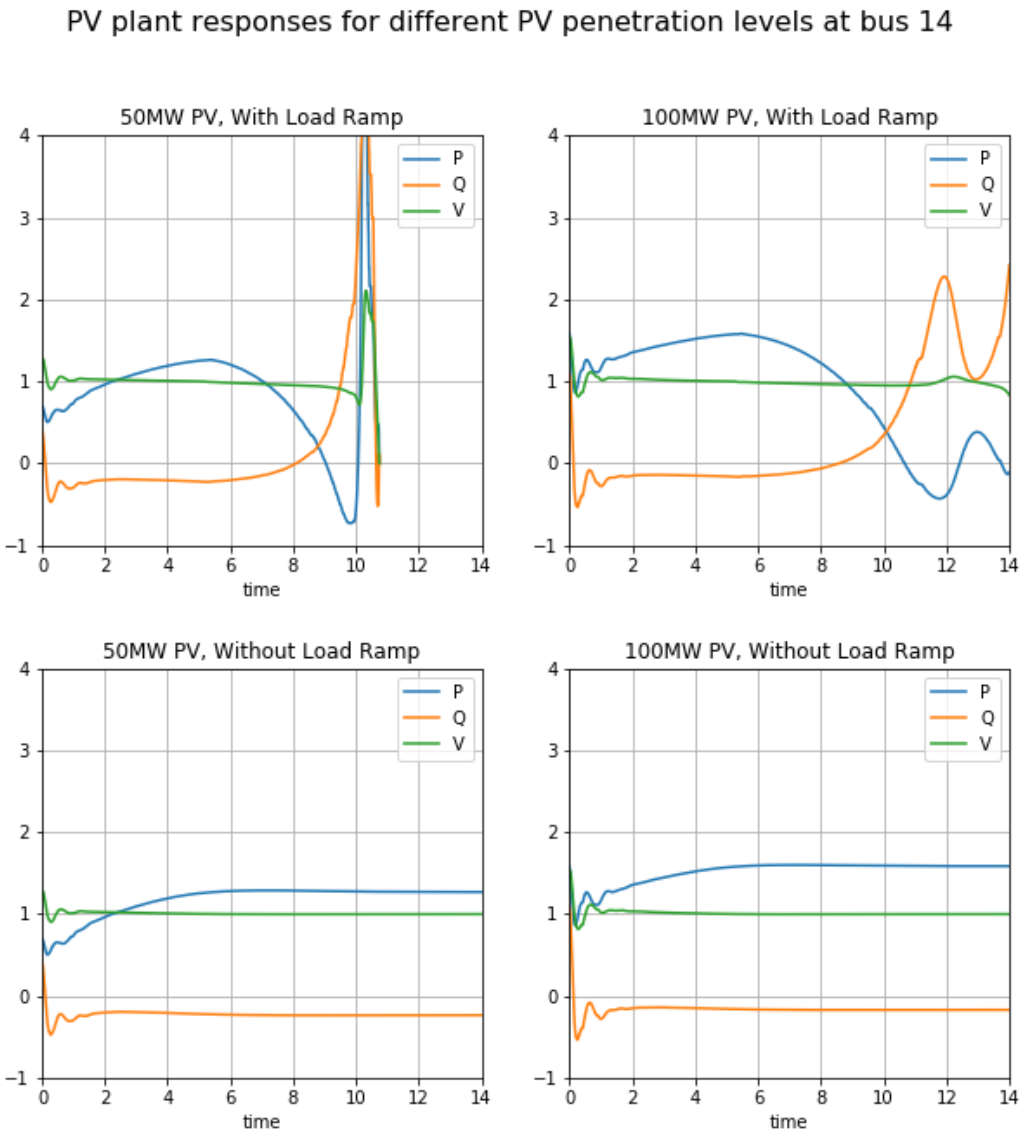

Figure 30: PV plant's response to various penetration level on bus 14

4 Conclusions and Future Work

4.1 Conclusions

This thesis presents the assessment of the effect of Distributed Energy Resources in a transmission system using steady-state voltage stability analysis of transmission lines. For this purpose, the IEEE 14 bus test model was analyzed using both DEW and OpenModelica as described in Sections 3.1 and 3.2, respectively.

The steady-state analysis is performed using a GTA-based power flow solver in DEW. Maximum loading levels at the load buses are calculated using this power flow solver, and the stability margins of transmission lines are calculated using the voltage stability index in DEW as derived in Equation 17. In section 3.1.2, baseload margins at individual bus levels are calculated and presented. After identifying maximum loadability, the loading level on a particular bus is increased to the maximum level until the voltage stability margin of one of the lines approaches zero. This process is repeated for all the load buses in the network. These localized loadings (as presented in Table 1) are later used to calculate stability margins of the transmission lines across the entire system, which is shown in Table 2 in the form of a voltage stability heat map. The heat map helps visualize the impact on transmission line segments due to increased loading at corresponding buses. A loadability index (λ) is calculated to sort the buses, and the resulting order is used to identify the weak links in the system. From the heat map, bus 03 is the weakest bus in the system in terms of voltage stability index calculated at all the transmission lines. It is also demonstrated that the increased loading on the system leads to a decrease in the stability margin of the transmission lines due to reduced voltage levels at load points.

Two scenarios have been studied with a PV plant added at weaker buses- bus 03 and bus 14 to assess the effect of PV penetration in the system. The first scenario observes the PV generation's effects at 10%, 20%, and 40% penetration levels on bus 03. The result shows that the lines' voltage stability margins improve upon the addition of the PV plant. However, the loss of the PV plant on bus 03 caused the stability margin of line 02-03 to approach zero, at which the system goes unstable. This observation in the steady-state analysis is verified later in the dynamic simulation.

The second scenario involves the addition of a PV plant on load bus 14. The rating of the PV plant is kept the same as in bus 03 in the previous case. This experiment considers only the line segments that connect bus 14 to the substation. The voltage stability margins and loading levels of these lines are calculated. The relationship between them is found to be linear in the 0-90% loading level. A regression equation is

developed using the lines' loading levels as y-parameter and voltage stability margins as x-parameter. The slope of this equation gives the sensitivity, which is defined as the ratio of change in loading to the change in stability margin, and the intercept gives the initial loading. This equation can be used to calculate a new loading level per unit change in the stability margin of the transmission lines. The relationship between the bus voltage and the line loadings can be established both with and without a PV plant. The result presented in Table 3 shows the increased loadability with the addition of PV generation. However, the expansion of PV has also resulted in increased sensitivity on lines adjacent to the PV location. Since the sensitivity affects the rate of change in loadability per unit change in stability margin, reduced sensitivity leads to the system's reduced capability to remain stable against heavy load switching events. In this case, the load margin at line 03-04 is reduced while the margin at line 09-14 is increased as PV is added to bus 14. This is the example case where the PV generation added on a bus affects another location in the system, moving the system towards instability. This information can be crucial during the planning phase of DER integration and the operation with renewable generation.

In the dynamic simulation, the experiment performed are similar to that in the steady-state analysis. The PV plants added to bus 03 and bus 14 are simulated with varying penetration levels- 0 MW, 50 MW, and 100 MW. The PV addition to bus 03 shows an improvement in the system's stability; however, the PV addition at bus 14 decreases its stability. This example case at bus 14 shows that as more PV plants are added further away from generation, the complexity increases for dynamic reactive power support during voltage excursions. The challenge for fast frequency response and inertial response also increases in these situations and can easily cause system instability if failed to address these issues. When significant amounts of DER and loads are present, even a momentary loss of DER on some buses will exacerbate the weaker bus's stress and trigger the system to collapse.

4.2 Future Work

Future work can combine contingency analysis and optimization techniques to minimize the impact of generation loss. These analyses can be combined with sizing and location techniques to include the method in this thesis to generate stability heat maps, which help to relate the effect of specific buses to specific lines in the system. Thus, the data can be analyzed using statistical approaches, and extensive data set modeling can be employed to observe one bus's effect on the entire system.

Future work could also address using the system state that exists as the stability margin approaches zero to initialize the dynamic analysis instead of the ramping of the load as used in this work.

Bibliography

[1] P. Kundur, N. J. Balu, and M. G. Lauby, *Power system stability and control*. New York: McGraw-Hill, 1994.

[2] S. Lumbreras and A. Ramos, "Chapter 7 - Better Transmission Networks for a Smarter Global System," in *Pathways to a Smarter Power System*, A. Taşcıkaraoğlu and O. Erdinç, Eds. Academic Press, 2019, pp. 205–223.

[3] M. Esmaili, "Placement of minimum distributed generation units observing power losses and voltage stability with network constraints," *Transmission Distribution IET Generation*, vol. 7, no. 8, pp. 813–821, Aug. 2013, doi: 10.1049/iet-gtd.2013.0140.

[4] M. Gautam, N. Bhusal, M. Benidris, C. Singh, and J. Mitra, "A Sensitivity-based Approach for Optimal Siting of Distributed Energy Resources," in *2020 International Conference on Probabilistic Methods Applied to Power Systems (PMAPS)*, Aug. 2020, pp. 1–6, doi: 10.1109/PMAPS47429.2020.9183471.

[5] S. Eftekharnejad, V. Vittal, G. T. Heydt, B. Keel, and J. Loehr, "Impact of increased penetration of photovoltaic generation on power systems," *IEEE Transactions on Power Systems*, vol. 28, no. 2, pp. 893–901, May 2013, doi: 10.1109/TPWRS.2012.2216294.

[6] National Renewable Energy Laboratory (NREL), Golden, CO., "Reliable, Low Cost Distributed Generator/Utility System Interconnect: 2001 Annual Report," NREL/SR-560-34634, 15004475, Aug. 2003. doi: 10.2172/15004475.

[7] H. Liu, L. Jin, D. Le, and A. A. Chowdhury, "Impact of high penetration of solar photovoltaic generation on power system small signal stability," in *2010 International Conference on Power System Technology*, Oct. 2010, pp. 1–7, doi: 10.1109/POWERCON.2010.5666627.

[8] Y. Zhang, C. Mensah-Bonsu, P. Walke, S. Arora, and J. Pierce, "Transient over-voltages in high voltage grid-connected PV solar interconnection," in *IEEE PES General Meeting*, Jul. 2010, pp. 1–6, doi: 10.1109/PES.2010.5589731.

[9] R. Toma and M. Gavrilas, "The impact on voltage stability of the integration of renewable energy sources into the electricity grids," in *2014 International Conference and Exposition on Electrical and Power Engineering (EPE)*, Oct. 2014, pp. 1051–1054, doi: 10.1109/ICEPE.2014.6970069.

[10] V. Widiputra, J. Kong, Y. Yang, J. Jung, and R. Broadwater, "Maximizing Distributed Energy Resource Hosting Capacity of Power System in South Korea Using Integrated Feeder, Distribution, and Transmission System," *Energies*, vol. 13, no. 13, p. 3367, Jul. 2020, doi: 10.3390/en13133367.

[11] B. A. Bhatti, R. Broadwater, and M. Dilek, "Analyzing Impact of Distributed PV Generation on Integrated Transmission & Distribution System Voltage

Stability—A Graph Trace Analysis Based Approach," *Energies*, vol. 13, no. 17, Art. no. 17, Jan. 2020, doi: 10.3390/en13174526.

[12] P. Shrestha, "Inverter-based Control to Enhance the Resiliency of a Distribution System," Thesis, Virginia Tech, 2019.

[13] N. Bhusal, M. Abdelmalak, M. Kamruzzaman, and M. Benidris, "Power System Resilience: Current Practices, Challenges, and Future Directions," *IEEE Access*, vol. 8, pp. 18064–18086, 2020, doi: 10.1109/ACCESS.2020.2968586.

[14] N. Bhusal, M. Gautam, and M. Benidris, "Sizing of Movable Energy Resources for Service Restoration and Reliability Enhancement," in *2020 IEEE Power Energy Society General Meeting (PESGM)*, Aug. 2020, pp. 1–5, doi: 10.1109/PESGM41954.2020.9281558.

[15] R. P. Broadwater, A. Chandrasekaran, C. T. Huddleston, and A. H. Khan, "Power flow analysis of unbalanced multiphase radial distribution systems," *Electric Power Systems Research*, vol. 14, no. 1, pp. 23–33, Feb. 1988, doi: 10.1016/0378-7796(88)90044-2.

[16] A. Tbaileh, H. Jain, R. Broadwater, J. Cordova, R. Arghandeh, and M. Dilek, "Graph Trace Analysis: An object-oriented power flow, verifications and comparisons," *Electric Power Systems Research*, vol. 147, pp. 145–153, Jun. 2017, doi: 10.1016/j.epsr.2017.02.034.

[17] H. Jain, "Dynamic Simulation of Power Systems using Three Phase Integrated Transmission and Distribution System Models: Case Study Comparisons with Traditional Analysis Methods," p. 158.

[18] R. P. Broadwater, S. Rahman, H. E. Shaalan, and R. E. Lee, "A distribution engineering workstation for undergraduate and graduate education," *IEEE Transactions on Power Systems*, vol. 8, no. 4, pp. 1385–1391, Nov. 1993, doi: 10.1109/59.260937.

[19] P. Kundur *et al.*, "Definition and classification of power system stability IEEE/CIGRE joint task force on stability terms and definitions," *IEEE Transactions on Power Systems*, vol. 19, no. 3, pp. 1387–1401, Aug. 2004, doi: 10.1109/TPWRS.2004.825981.

[20] I. Musirin and T. K. Abdul Rahman, "Novel fast voltage stability index (FVSI) for voltage stability analysis in power transmission system," in *Student Conference on Research and Development*, Jul. 2002, pp. 265–268, doi: 10.1109/SCORED.2002.1033108.